Quantum Chromodynamics

Rene Poncelet

September 8, 2026

Contents

Preamble

These lecture notes were prepared for the Herbstschule HEP taking place in Bad Honnef from 1st to 11th of September 2026. This lecture is a crash course in QCD, ranging from basics to LHC phenomenology.

This lecture is phenomenologically oriented, meaning we will focus on the theoretical aspects most relevant to making precise predictions for QCD observables at the LHC. Due to time constraints, we will not be able to dive deeply into the theoretical foundations behind many of the topics we discuss. Radiative corrections, in particular, are crucial to LHC phenomenology but also a highly technical topic. The lecture aims to review the most important aspects but may be too shallow for interested readers; we point to the existing excellent literature on QCD and related subjects, for example [1, 2, 3, 4].

1 Introduction

In the post-Higgs-discovery age, one of the main targets of particle physics remains: to look for signatures that cannot be explained within the Standard Model of Particle physics (SM). We expect the SM to be incomplete, an effective theory if one wishes so, because we have evidence for phenomena outside of particle physics, in particular astrophysics and cosmology, that go beyond the standard framework of the SM and general relativity. This includes the observed matter-antimatter imbalance, evidence for dark matter and dark energy, and the unclear nature of neutrino masses.

However, starting from the perspective that the SM is incredibly successful in describing collision data collected at the LHC (see the ATLAS SM summary in Fig. 1) and its predecessors, we have to look out for very subtle effects implied by new interactions or particles, or require exploring extreme corners of the phase space[1]. This can take the form of precision measurements of SM quantities, which are interesting for their own sake but also in order to hunt for inconsistencies, or, for example, global fits of effective field theories describing heavy new physics. Both approaches require a high-fidelity understanding of SM backgrounds (foregrounds would be the better word).

The SM is a *complicated* theory model. We can't produce exact predictions in general (except for some quite general symmetry-based predictions), especially not for high-energy scattering experiments with high-multiplicity final states. In the limit of small coupling, perturbative methods allow us to make systematic approximations of transition amplitudes and, by that, of cross sections. This underpins the success of QFT, for example in QED. QCD, the theory of the strong force, is however strongly coupled at low energies, and perturbative methods apply only at very high energies, and non-perturbative as well as all-order effects are important. At low energy, lattice QCD can provide non-perturbative results by discretizing path integrals. Although very powerful, it is currently infeasible to use at high energy, because the number of lattice points is inversely proportional to the energy scale.

In practice, we need approximations that introduce theoretical uncertainties. In the best case, we can systematically improve the approximation and thus the precision/accuracy of the predictions. This is the case for perturbative methods, for example fixed-order perturbation theory, resummation, and parton showering. In some cases this

[1]Of course, if there is a new resonance directly produced in the bulk of the phase space, the whole picture would change. So far we don't see anything directly produced in bulk, and the HL-LHC, with essentially the same phase space as the LHC, will not drastically change this.

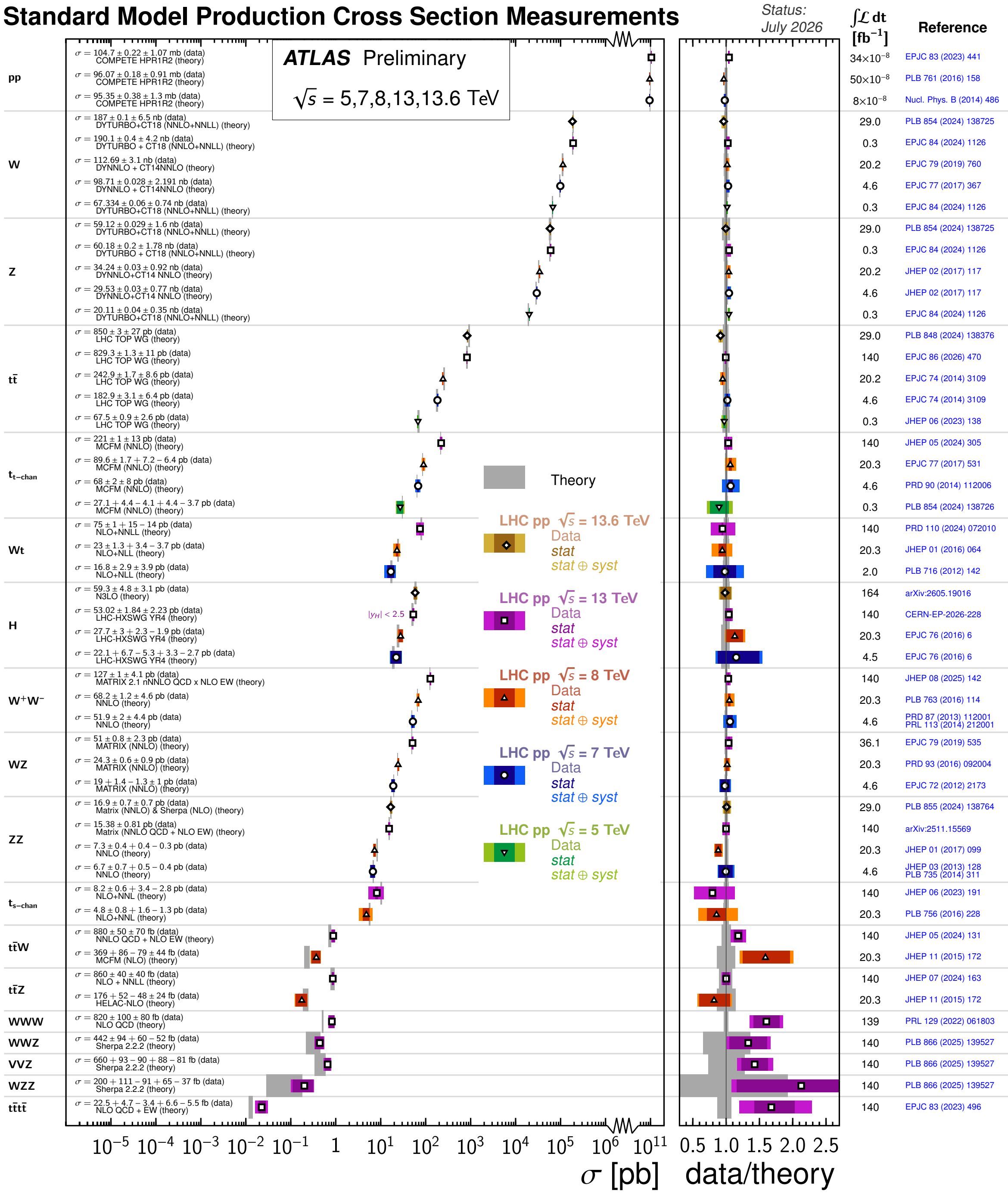

Figure 1: ATLAS SM measurement summary plot [5].

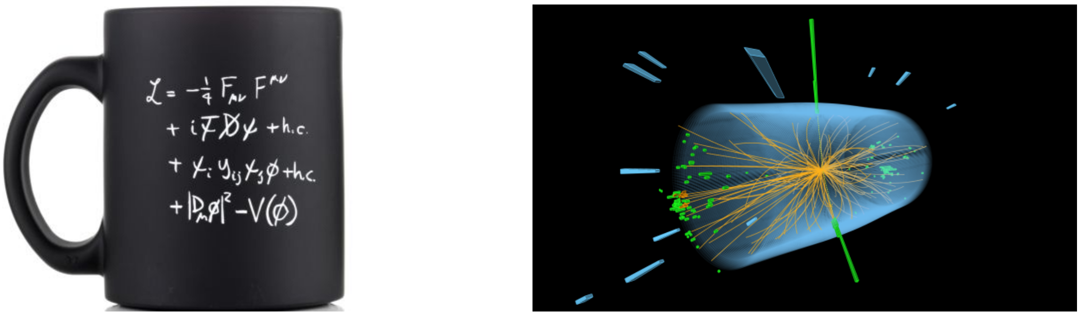

Figure 2: Theory vs Real World

is not the case (often the non-perturbative parts of calculations), and we must hope that their impact is small for the physics of interest or can at least be systematically assessed.

Modern collider physics relies fundamentally on General-Purpose Monte Carlo event generators (notably Pythia 8, Herwig 7, and Sherpa 3). They serve as the computational bridge connecting (Fig. 2):

1. **The Theory World:** The Standard Model Lagrangian $\mathcal{L}_{\text{SM}}$, gauge symmetries, and perturbative Feynman amplitude calculations.

2. **The Real World:** Hundreds of collimated, detectable color-singlet hadrons, leptons, and photons measured inside detectors such as ATLAS and CMS.

Monte Carlo event generators combine systematically improvable parts (fixed-order, resummation/parton-shower) with phenomenological models for non-perturbative physics (Fig. 3). This combination exploits scale factorization to separate the important degrees of freedom at different stages of the simulations:

"What you see depends on the resolution scale."

Due to the asymptotic freedom of Quantum Chromodynamics (QCD), the strong coupling constant $\alpha_s(Q^2)$ runs as:

$$\alpha_s(\mu^2) = \frac{\alpha_s(\mu_0^2)}{1 + b_0 \alpha_s(\mu_0^2) \ln(\mu^2/\mu_0^2)}, \qquad b_0 = \frac{11 C_A - 2 n_f}{12\pi}. \tag{1}$$

This allows a systematic decomposition into four primary physical domains across decreasing energy scales (Q):

- **Hard Scattering ($Q \gg \Lambda_{\text{QCD}}$):** High momentum transfer, evaluated with fixed-order perturbation theory. Here the coupling is small, $\alpha_s(m_Z) \approx 0.118$.

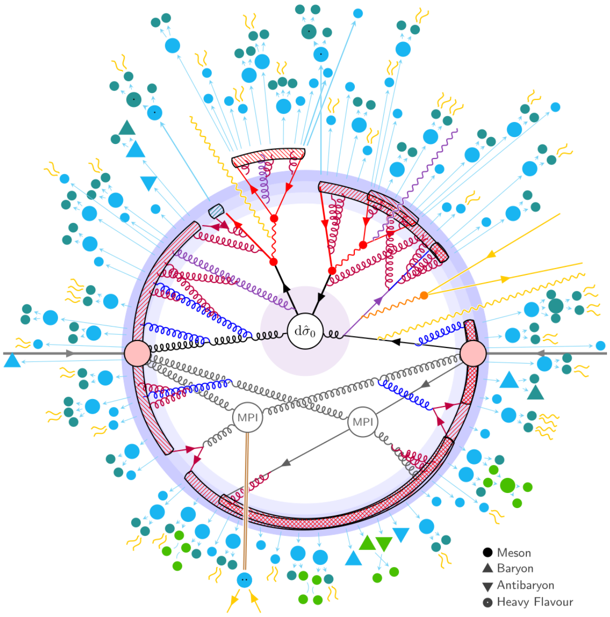

Figure 3: Pythia [<**empty citation**>] representation of a simulated event.

- **Parton Shower (1 GeV $\lesssim Q \lesssim \mu_F$):** Multiple soft and collinear branchings, evaluated with all-orders logarithmic resummation. This covers the regime down to scales where the strong coupling becomes non-perturbative.
- **Matching/Merging:** Eliminating double counting and phase-space gaps between fixed-order and resummed/showered predictions.
- **Hadronization & Beam Remnants ($Q \sim \Lambda_{\text{QCD}}$):** Non-perturbative confinement models (color-reconnection, fragmentation) and multi-parton interactions.

We begin our discussion of QCD with a short history and the construction of the theory in section 2. We introduce the means for calculations beyond tree-level approximations in perturbative QCD in section 3. The discussion of hadrons in the initial state and thus parton-distribution functions follows in section 4. We then discuss multiple emissions and resummation in section **??**. Equipped with all necessary ingredients, we will close the lecture in section **??** with a phenomenology discussion at the LHC.

2 Basics

This section introduces QCD and provides the starting point for perturbative calculations, as well as some more advanced concepts later on. During the lecture, we will skim over many details, and the notes will serve more as a reference for discussion.

2.1 A bit of history: experimental evidence for QCD

2.1.1 Experimental Evidence for Quarks

2.1.2 Experimental Evidence for the Color Degree of Freedom

Quantum Chromodynamics (QCD) is the non-Abelian $SU(3)$ gauge theory governing the strong interaction among quarks and gluons. The introduction of the internal degree of freedom termed *color* ($N_c = 3$) is mandated by several critical experimental and theoretical observations:

1. **Spin-Statistics Paradox of the Δ^{++} Baryon:**
   The Δ^{++} baryon has spin $J = 3/2$ and electric charge $+2$, comprising three up quarks (uuu). In its ground state ($L = 0$), its spatial wavefunction ψ_{space}, spin state $\chi_{\text{spin}} = |\uparrow\uparrow\uparrow\rangle$, and flavor state $\phi_{\text{flavor}} = |uuu\rangle$ are all symmetric under particle exchange:
   $$|\Delta^{++}\rangle_{\text{total}} = \psi_{\text{space}} \otimes \chi_{\text{spin}} \otimes \phi_{\text{flavor}} \otimes \xi_{\text{color}}. \tag{2}$$
   Since quarks are Dirac fermions, Fermi-Dirac statistics require the overall state to be totally antisymmetric. Thus, an exact $SU(3)$ color singlet representation must exist:
   $$\xi_{\text{color}} = \frac{1}{\sqrt{6}}\epsilon^{ijk}|q_i q_j q_k\rangle \quad (i, j, k \in \{1, 2, 3\}). \tag{3}$$
2. **The R-ratio in e^+e^- Annihilation:**
   At leading order (LO) in the parton model, the ratio of the total hadronic cross-section to the muon pair cross-section in e^+e^- collisions measures the sum over all active quark color-spin states:
   $$R \equiv \frac{\sigma(e^+e^- \to \text{hadrons})}{\sigma(e^+e^- \to \mu^+\mu^-)} = N_c \sum_f Q_f^2, \tag{4}$$
   where Q_f is the electric charge of quark flavor f in units of the positron charge e.

   - Below the charm threshold (u, d, s active):
     $$R = 3 \times \left[\left(\frac{2}{3}\right)^2 + \left(-\frac{1}{3}\right)^2 + \left(-\frac{1}{3}\right)^2\right] = 3 \times \frac{6}{9} = 2. \tag{5}$$

- Above the bottom threshold (u, d, s, c, b active):

$$R = 3 \times \left(\frac{4}{9} + \frac{1}{9} + \frac{1}{9} + \frac{4}{9} + \frac{1}{9} \right) = \frac{11}{3} \approx 3.67. \tag{6}$$

3. **Neutral Pion Decay ($\pi^0 \to \gamma\gamma$):**
   From the axial anomaly (ABJ anomaly) in QED, the decay width is given by:

$$\Gamma(\pi^0 \to \gamma\gamma) = \left(\frac{N_c}{3} \right)^2 \frac{\alpha_{\rm em}^2 m_\pi^3}{64\pi^3 f_\pi^2} \approx 7.73 \text{ eV} \quad (\text{for } N_c = 3), \tag{7}$$

matching experimental measurements with sub-percent precision.

2.2 The QCD Lagrangian and Feynman rules

2.2.1 The Non-Abelian SU(3) Gauge Theory

Quark fields transform under the fundamental representation ($\mathbf{3}$) of the local gauge group $SU(3)_c$:

$$\psi(x) \to \psi'(x) = U(x)\psi(x) = \exp\left(ig_s\theta^a(x)T^a\right)\psi(x), \tag{8}$$

where T^a ($a = 1, \dots, 8$) are the 8 generators of the Lie algebra $\mathfrak{su}(3)$ satisfying:

$$[T^a, T^b] = if^{abc}T^c. \tag{9}$$

The gauge-covariant derivative acting on quarks is:

$$D_\mu = \partial_\mu - ig_s T^a A^a_\mu, \tag{10}$$

where A^a_μ are the 8 non-Abelian gluon gauge fields transforming in the adjoint representation ($\mathbf{8}$).

The non-Abelian field strength tensor $F^a_{\mu\nu}$ is defined through the commutator of covariant derivatives:

$$[D_\mu, D_\nu] = -ig_s T^a F^a_{\mu\nu} \implies F^a_{\mu\nu} = \partial_\mu A^a_\nu - \partial_\nu A^a_\mu + g_s f^{abc} A^b_\mu A^c_\nu. \tag{11}$$

The classical, gauge-invariant QCD Lagrangian density is:

$$\mathcal{L}_{\rm QCD} = -\frac{1}{4} F^a_{\mu\nu} F^{a\mu\nu} + \sum_{f=1}^{n_f} \bar{\psi}_{f,i}(i\not{D}_{ij} - m_f\delta_{ij})\psi_{f,j}. \tag{12}$$

The quadratic term in $F^a_{\mu\nu}$ gives rise to cubic ($g_s f^{abc}$) and quartic ($g_s^2 f^{abe} f^{cde}$) gluon self-interactions, leading directly to the phenomenon of asymptotic freedom.

2.2.2 Color Algebra, Representation Invariants, and Fierz Identity

The standard representation uses Gell-Mann matrices: $T^a = \frac{1}{2}\lambda^a$:

$$\lambda^1 = \begin{pmatrix} 0 & 1 & 0 \\ 1 & 0 & 0 \\ 0 & 0 & 0 \end{pmatrix} \quad \lambda^2 = \begin{pmatrix} 0 & i & 0 \\ -i & 0 & 0 \\ 0 & 0 & 0 \end{pmatrix} \quad \lambda^3 = \begin{pmatrix} 1 & 0 & 0 \\ 0 & -1 & 0 \\ 0 & 0 & 0 \end{pmatrix} \quad \lambda^4 = \begin{pmatrix} 0 & 0 & 1 \\ 0 & 0 & 0 \\ 1 & 0 & 0 \end{pmatrix}$$

$$\lambda^5 = \begin{pmatrix} 0 & 0 & -i \\ 0 & 0 & 0 \\ i & 0 & 0 \end{pmatrix} \quad \lambda^6 = \begin{pmatrix} 0 & 0 & 0 \\ 0 & 0 & 1 \\ 0 & 1 & 0 \end{pmatrix} \quad \lambda^7 = \begin{pmatrix} 0 & 0 & 0 \\ 0 & 0 & 1 \\ 0 & 1 & 0 \end{pmatrix} \quad \lambda^8 = \frac{1}{\sqrt{3}} \begin{pmatrix} 1 & 0 & 0 \\ 0 & 1 & 0 \\ 0 & 0 & 2 \end{pmatrix}$$

The core group-theoretical constants are:

- **Fundamental Index (T_F):**

$$\mathrm{Tr}(T^a T^b) = T_F \delta^{ab}, \quad T_F = \frac{1}{2}. \tag{13}$$

- **Fundamental Casimir (C_F):**

$$(T^a T^a)_{ij} = C_F \delta_{ij}, \quad C_F = \frac{N_c^2 - 1}{2N_c} = \frac{3^2 - 1}{2 \times 3} = \frac{4}{3}. \tag{14}$$

- **Adjoint Casimir (C_A):**

$$f^{acd} f^{bcd} = C_A \delta^{ab}, \quad C_A = N_c = 3. \tag{15}$$

- **Fierz Completeness Identity:**

$$T^a_{ij} T^a_{kl} = \frac{1}{2} \left(\delta_{il}\delta_{jk} - \frac{1}{N_c} \delta_{ij}\delta_{kl} \right). \tag{16}$$

- **Color Trace Representation of Structure Constants:**

$$\mathrm{Tr}(T^a T^b T^c) - \mathrm{Tr}(T^c T^b T^a) = i T_F f^{abc} = \frac{i}{2} f^{abc} \tag{17}$$

2.2.3 Gauge choices

In non-Abelian gauge theories ($SU(N)$ or $SU(2)_L \times U(1)_Y$), the path integral over gauge configurations,

$$Z = \int \mathcal{D}A \, \exp\left(i \int \mathrm{d}^4 x \, \mathcal{L}_{\mathrm{inv}}[A] \right), \tag{18}$$

is ill-defined because the gauge-invariant action $\mathcal{L}_{\mathrm{inv}}[A]$ is flat along gauge orbits generated by transformations $A_\mu \to A_\mu^\alpha$. Integrating along these non-physical, infinitely redundant orbits makes the functional measure diverge and renders the gauge-field propagator non-invertible. Another, less formal, way to see that is to look into perturbation theory. An issue can be seen when looking at the action in momentum space:

$$S_{\mathrm{YM}} = i \int \mathrm{d}^4 x \left\{ -\frac{1}{4} F^a_{\mu\nu} F^{a,\mu\nu} \right\} \ni \frac{i}{2} \int \mathrm{d}^4 x A^a_\mu (\partial^2 g^{\mu\nu} - \partial^\mu \partial^\nu) A^b_\nu \delta_{ab} \tag{19}$$

In perturbation theory, i.e., the derivation of the Feynman rules, the A fields' propagator is the inverse of the bilinear form, i.e.:

$$i\Delta_{\mu\rho} \left(p^2 g^{\rho\nu} - p^\rho p^\nu \right) = g^\nu_\mu \tag{20}$$

but we can easily see:

$$i\Delta_{\mu\rho} \left(p^2 g^{\rho\nu} - p^\rho p^\nu \right) p_\nu = 0 \neq p_\mu \tag{21}$$

The main reason for this issue is that too many degrees of freedom propagate. A possibility to solve it is to use a local gauge transformation to eliminate it; this procedure is called gauge fixing.

In general, gauge fixing can be implemented through Lagrange multipliers on the Lagrangian level. Two broad classes of gauges are commonly used. The covariant gauges, or R_ξ-gauges (I will use λ or ξ as the Lagrange parameter), use the additional constraint

$$\partial \mathcal{A} = 0 \quad \rightarrow \mathcal{L}_{\mathrm{GF}} = -\frac{1}{2\lambda} \left(\partial_\mu \mathcal{A}^\mu \right)^2 \;\; \lambda \in \mathbb{R} \tag{22}$$

This leads to an additional term in the bilinear form, and we can find the inverse easily:

$$i\Delta_{\mu\rho} \left(p^2 g^{\rho\nu} - (1 - \frac{1}{\lambda}) p^\rho p^\nu \right) = g^\nu_\mu \tag{23}$$

$$\Rightarrow \Delta_{\mu\nu} = \frac{-i}{p^2 + i\epsilon} \left[g_{\mu\nu} - (1 - \lambda) \frac{p^\mu p^\nu}{p^2} \right] \tag{24}$$

While this yields an invertible propagator, it also allows non-transverse degrees of freedom to propagate. The Faddeev-Popov procedure introduces ghost particles that precisely cancel these contributions (see the short discussion below). In any case, the propagator depends on the additional parameter λ, the physical results (i.e. matrix elements) do not depend on it (super useful for cross checks). Famous choices are $\lambda = 1$ (Feynman gauge) and $\lambda = 0$ (Landau gauge).

The other option are physical gauges $n_\mu A^\mu = 0$ where $n \cdot p \neq 0$, where n is an arbitrary vector. The choice $n^2 = 0$ is called light-cone gauge. Again implemented through Lagrange multipliers:

$$\mathcal{L}_{\mathrm{GF}} = -\frac{1}{2\lambda} \left(n_\mu \mathcal{A}^\mu \right)^2 \tag{25}$$

which leads to the propagator:

$$\Delta_{\mu\nu}(p,n) = \frac{-i}{p^2 + i\epsilon}\left[g_{\mu\nu} - \frac{p_\mu n_\nu + p_\nu n_\mu}{p\cdot n} + \frac{n^2 p_\mu p_\nu}{(p\cdot n)^2}\right]. \tag{26}$$

Here, the final matrix elements are again independent of n. In this case, no ghost particles are interacting with the gauge field, and thus they can be integrated out from the Lagrangian and do not appear in the final expressions.

Extra: The Faddeev-Popov Procedure and Ghosts To integrate over physical configurations only, we insert a gauge-fixing condition $G^a(A) = 0$ (e.g., covariant gauge $G^a(A) = \partial^\mu A^a_\mu$) using the identity resolution:

$$1 = \Delta_{\rm FP}[A] \int \mathcal{D}\alpha\, \delta\left(G^a(A^\alpha)\right), \tag{27}$$

where $\Delta_{\rm FP}[A] = \det\left(\frac{\delta G^a(A^\alpha)}{\delta\alpha^b}\right)$ is the Faddeev-Popov determinant.

Factoring out the infinite volume of the gauge group $\int \mathcal{D}\alpha$, the effective path integral becomes:

$$Z = \int \mathcal{D}A\, \Delta_{\rm FP}[A]\, \delta\left(G^a(A)\right) \exp\left(i\int \mathrm{d}^4x\, \mathcal{L}_{\rm inv}[A]\right). \tag{28}$$

By shifting the condition to $G^a(A) = \omega^a(x)$ and performing a Gaussian functional integration over $\omega^a(x)$ with width parameter ξ, we generate the standard covariant gauge-fixing term:

$$\mathcal{L}_{\rm gf} = -\frac{1}{2\xi}\left(G^a(A)\right)^2 = -\frac{1}{2\xi}(\partial^\mu A^a_\mu)(\partial^\nu A^a_\nu). \tag{29}$$

The determinant $\det\left(\frac{\delta G^a}{\delta\alpha^b}\right)$ is exponentiated into the Lagrangian by introducing anti-commuting scalar fields $c^a, \bar{c}^a$ (Faddeev-Popov ghosts and antighosts):

$$\Delta_{\rm FP}[A] = \int \mathcal{D}c\,\mathcal{D}\bar{c}\, \exp\left(i\int \mathrm{d}^4x\, \mathcal{L}_{\rm ghost}\right), \tag{30}$$

where for Yang-Mills gauge theory in covariant gauges:

$$\frac{\delta G^a(A^\alpha)}{\delta\alpha^b} = -\frac{1}{g}\partial^\mu D^{ab}_\mu = -\frac{1}{g}\left(\delta^{ab}\partial^2 - gf^{abc}\partial^\mu A^c_\mu\right). \tag{31}$$

Absorbing constant normalization factors, the ghost Lagrangian reads:

$$\mathcal{L}_{\rm ghost} = -\bar{c}^a\partial^\mu D^{ab}_\mu c^b = \bar{c}^a(-\partial^2\delta^{ab} - gf^{abc}\partial^\mu A^c_\mu)c^b. \tag{32}$$

In physical gauges $\partial A = 0$ and the ghost fields decouple.

2.2.4 Faddeev-Popov Ghosts

As we saw in the section on the EW theory, we need gauge fixing to derive gauge-boson propagators. In covariant R_ξ gauges:

$$\mathcal{L}_{\text{gf}} = -\frac{1}{2\xi}(\partial^\mu A^a_\mu)^2. \tag{33}$$

The corresponding Faddeev-Popov determinant introduces anticommuting scalar fields (ghosts $c^a, \bar{c}^a$) transforming in the adjoint representation:

$$\mathcal{L}_{\text{ghost}} = \bar{c}^a(-\partial^\mu D^{ab}_\mu)c^b = \bar{c}^a\left(-\partial^2\delta^{ab} - g_s f^{abc}\partial^\mu A^c_\mu\right)c^b. \tag{34}$$

Ghosts cancel the contributions of unphysical timelike and longitudinal gluon polarizations in loop amplitudes.

2.3 QCD Feynman Rules

All momenta are defined flowing **into** the vertices unless explicitly indicated otherwise. Fundamental color indices are denoted by $i, j \in \{1, \ldots, N_c\}$, and adjoint gluon color indices by $a, b, c, d \in \{1, \ldots, N_c^2 - 1\}$.

Propagators

Field / Line	**Feynman Graph**	**Propagator Expression**
Quark (q)	$j \xrightarrow{p} i$	$\delta_{ij}\dfrac{i(\not{p}+m)}{p^2 - m^2 + i\epsilon}$
Gluon (A^a_μ) *Cov.* R_ξ	$a,\mu \overset{p}{\rightsquigarrow} b,\nu$	$\dfrac{-i\delta^{ab}}{p^2+i\epsilon}\left[g^{\mu\nu} - (1-\xi)\dfrac{p^\mu p^\nu}{p^2}\right]$ ($\xi = 1$ for Feynman Gauge)
Gluon (A^a_μ) *Axial* ($n \cdot A = 0$)	$a,\mu \overset{p}{\rightsquigarrow} b,\nu$	$\dfrac{-i\delta^{ab}}{p^2+i\epsilon}\left[g^{\mu\nu} - \dfrac{n^\mu p^\nu + n^\nu p^\mu}{n\cdot p} + \dfrac{n^2 p^\mu p^\nu}{(n\cdot p)^2}\right]$
Ghost (c^a)	$b \overset{p}{\dashrightarrow} a$	$\delta^{ab}\dfrac{i}{p^2+i\epsilon}$

Vertices

Vertex	Feynman Graph	Feynman Rule
Quark-Gluon	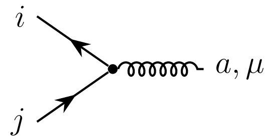	$-ig_s(T^a)_{ij}\gamma^\mu$
Ghost-Gluon	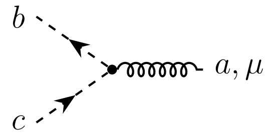	$-g_s f^{abc} p^\mu$ (p is the outgoing ghost momentum)
3-Gluon Vertex	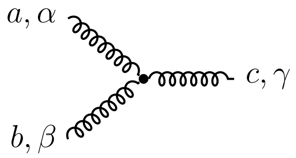	$-g_s f^{abc} V_{\alpha\beta\gamma}(p, q, r)$
4-Gluon Vertex	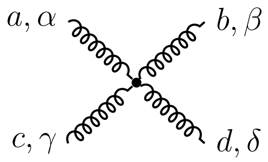	$-ig_s^2\Big[f^{xac}f^{xbd}(g_{\alpha\beta}g_{\gamma\delta} - g_{\alpha\delta}g_{\beta\gamma})$ $+f^{xad}f^{xcb}(g_{\alpha\gamma}g_{\beta\delta} - g_{\alpha\beta}g_{\gamma\delta})$ $+f^{xab}f^{xdc}(g_{\alpha\delta}g_{\beta\gamma} - g_{\alpha\gamma}g_{\beta\delta})\Big]$

Define the canonical kinematic 3-boson tensor (all momenta incoming):

$$V_{\mu\nu\rho}(p_1, p_2, p_3) = (p_1 - p_2)_\rho g_{\mu\nu} + (p_2 - p_3)_\mu g_{\nu\rho} + (p_3 - p_1)_\nu g_{\rho\mu}$$

External Line Factors and Loop Rules

External Line	Factor	External Line	Factor
Incoming Fermion (s)	$u(p, s)$	Outgoing Fermion (s)	$\bar{u}(p, s)$
Incoming Anti-Fermion (s)	$\bar{v}(p, s)$	Outgoing Anti-Fermion (s)	$v(p, s)$
Incoming Vector Boson (λ)	$\varepsilon_\mu(p, \lambda)$	Outgoing Vector Boson (λ)	$\varepsilon^*_\mu(p, \lambda)$

- **Loop Integrals:** Integrate over every undetermined loop four-momentum k:

$$\int \frac{d^d k}{(2\pi)^d}$$

- **Fermion Loops:** Multiply by a factor of (-1) for each closed fermion loop.
- **Identical Fermions:** Multiply by a factor of (-1) for permutations/crossing of identical external fermions.
- **Symmetry Factors:** Divide by the combinatorial symmetry factor S for identical internal field configurations.

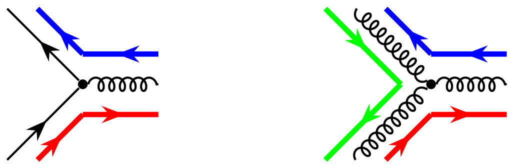

Figure 4: Example color flows

Colorflows In practice, the most convenient way to work with color charges is in terms of the identities in Equation 13 to Equation 17. The reason is that we do not observe 'open' charges in nature, and in all calculations we will sum over the color degrees of freedom, leading directly to expressions in terms of Casimirs or N_c.

Still, one might assign color flows[2] to Feynman diagrams; see, for example, Figure 4.

In this visualization, it becomes transparent that one can decompose Feynman diagrams into different flows, called the color flow basis, which describes the color structure in terms of color dipoles. Physically, we find that in certain kinematic limits, specific flows dominate the amplitudes or matrix elements, allowing systematic approximation.

2.4 Cross sections

Fermi's Golden Rule describes the transition probability between initial and final states. For an initial state containing either one decaying particle or two colliding beam particles, the physical observables (total/differential decay rates Γ and cross sections σ) factorize into three fundamental components:

1. A kinematic **flux / normalisation factor** (F or $2m$),
2. The Lorentz-invariant **matrix element squared** $|\mathcal{M}|^2$, averaged over initial internal degrees of freedom (spin, polarization, color) and summed over final states,
3. The **Lorentz-Invariant Phase Space (LIPS)** element $d\Phi_n$ for n final-state particles.

2.4.1 Lorentz-Invariant Phase Space (LIPS)

For n outgoing particles with four-momenta $p_1, p_2, \ldots, p_n$ and on-shell masses m_i ($p_i^2 = m_i^2$), the invariant n-body phase space measure $d\Phi_n(P \to \{p_i\})$ enforcing global four-

[2]The structure of the vertices in the fundamental/adjoint basis allows several color flows for one diagram.

momentum conservation is defined as:

$$d\Phi_n(P) = (2\pi)^4 \delta^{(4)}\left(P - \sum_{i=1}^{n} p_i\right) \prod_{i=1}^{n} \frac{d^3\vec{p}_i}{(2\pi)^3 2E_i}, \tag{35}$$

where $E_i = \sqrt{|\vec{p}_i|^2 + m_i^2}$. Equivalently, each single-particle phase space measure can be expressed in explicitly Lorentz-covariant four-momentum form:

$$\frac{d^3\vec{p}_i}{(2\pi)^3 2E_i} = \frac{d^4 p_i}{(2\pi)^4}\, \theta(p_i^0)\, 2\pi\delta(p_i^2 - m_i^2). \tag{36}$$

2.4.2 Scattering Cross Sections

For a two-body initial state $a(p_a) + b(p_b) \to 1(p_1) + 2(p_2) + \cdots + n(p_n)$, the master differential cross section is:

$$d\sigma = \frac{1}{F}\, |\mathcal{M}_{ab\to n}|^2\, d\Phi_n(p_a + p_b)\, S, \tag{37}$$

where:

- **Flux Factor (F):** The general, frame-independent Møller flux factor is given by:

$$F = 4\sqrt{(p_a \cdot p_b)^2 - m_a^2 m_b^2}. \tag{38}$$

In the **center-of-mass (CoM) frame** ($\vec{p}_a = -\vec{p}_b = \vec{p}_{\text{cm}}$, $\sqrt{s} = E_a + E_b$):

$$F = 4|\vec{p}_{\text{cm}}|\sqrt{s} = 4E_a E_b |v_a - v_b|. \tag{39}$$

In the **high-energy / massless limit** ($s \gg m_a^2, m_b^2$):

$$F \approx 4 p_a \cdot p_b = 2s. \tag{40}$$

- **Spin/Color-Averaged Matrix Element:** For initial states with discrete degeneracies n_a and n_b (e.g., $n_q = 2 \times N_c$ for spin and color degrees of freedom of a quark, or $n_g = 2 \times (N_c^2 - 1)$ for gluons):

$$|\mathcal{M}|^2 \equiv \langle \mathcal{M}|\mathcal{M}\rangle = \frac{1}{n_a n_b} \sum_{\text{spin, color}} \mathcal{M}(\text{spin,color})^* \mathcal{M}(\text{spin,color}). \tag{41}$$

- **Symmetry Factor (S):** If the final state contains k groups of identical, indistinguishable particles with multiplicities $n_1, n_2, \ldots, n_k$:

$$S = \prod_{j=1}^{k} \frac{1}{n_j!}. \tag{42}$$

2.4.3 Particle Decay Rates $(1 \to n)$

For the decay of an unstable single particle $a(P)$ of mass M in its rest frame $(P = (M, \vec{0}))$ into n particles:

$$d\Gamma = \frac{1}{2M} \left|\mathcal{M}_{a\to n}\right|^2 d\Phi_n(P)\, S, \tag{43}$$

where the matrix element is averaged over the initial polarization states of particle a.

The total decay width $\Gamma_{\text{tot}} = \sum_f \Gamma_f$ determines the mean lifetime $\tau = \hbar/\Gamma_{\text{tot}}$ and the Breit-Wigner resonance lineshape in the propagator.

2.5 Top-quark pairs, a tree-level example

At hadron colliders (such as the Tevatron and the LHC), top-quark pair production ($pp \to t\bar{t} + X$ or $p\bar{p} \to t\bar{t} + X$) at leading order (LO) in perturbative Quantum Chromodynamics (QCD) occurs via two partonic sub-processes:

1. **Quark-antiquark annihilation:** $q(p_1, i, s_1) + \bar{q}(p_2, j, s_2) \to t(p_3, k, s_3) + \bar{t}(p_4, l, s_4)$
2. **Gluon-gluon fusion:** $g(p_1, a, \lambda_1) + g(p_2, b, \lambda_2) \to t(p_3, k, s_3) + \bar{t}(p_4, l, s_4)$

Here $i, j, k, l \in \{1, \ldots, N_c\}$ denote fundamental $SU(N_c)$ color indices, $a, b \in \{1, \ldots, N_c^2 - 1\}$ denote adjoint color indices, and m_t is the on-shell top-quark mass. The incoming light quarks are treated as massless ($p_1^2 = p_2^2 = 0$), while the top quarks are on-shell:

$$p_3^2 = p_4^2 = m_t^2. \tag{44}$$

2.5.1 Mandelstam Invariants

The standard Mandelstam invariants for the $2 \to 2$ partonic system are defined as:

$$\hat{s} = (p_1 + p_2)^2 = 2p_1 \cdot p_2 = (p_3 + p_4)^2 = 2m_t^2 + 2p_3 \cdot p_4, \tag{45}$$

$$\hat{t} = (p_1 - p_3)^2 = m_t^2 - 2p_1 \cdot p_3 = (p_2 - p_4)^2 = m_t^2 - 2p_2 \cdot p_4, \tag{46}$$

$$\hat{u} = (p_1 - p_4)^2 = m_t^2 - 2p_1 \cdot p_4 = (p_2 - p_3)^2 = m_t^2 - 2p_2 \cdot p_3. \tag{47}$$

These satisfy the kinematic relation:

$$\hat{s} + \hat{t} + \hat{u} = 2m_t^2. \tag{48}$$

In the center-of-mass frame of the partonic collision, one can represent the invariants as a velocity $\beta = \sqrt{1 - \frac{4m_t^2}{\hat{s}}}$ and scattering angle θ:

$$\hat{t} = m_t^2 - \frac{\hat{s}}{2}(1 - \beta\cos\theta), \qquad \hat{u} = m_t^2 - \frac{\hat{s}}{2}(1 + \beta\cos\theta). \tag{49}$$

2.5.2 The Quark-Antiquark Annihilation Channel

At tree level, quark-antiquark annihilation is mediated by an s-channel gluon exchange:

$$i\mathcal{M}_{q\bar{q}\to t\bar{t}} = \left[\bar{v}_j(p_2)(-ig_s\gamma^\mu T^a_{ji})u_i(p_1)\right]\left(\frac{-ig_{\mu\nu}}{\hat{s}}\delta^{ab}\right)\left[\bar{u}_k(p_3)(-ig_s\gamma^\nu T^b_{kl})v_l(p_4)\right], \tag{50}$$

which simplifies to:

$$\mathcal{M}_{q\bar{q}\to t\bar{t}} = \frac{g_s^2}{\hat{s}}(T^a)_{ji}(T^a)_{kl}\left[\bar{v}(p_2)\gamma^\mu u(p_1)\right]\left[\bar{u}(p_3)\gamma_\mu v(p_4)\right]. \tag{51}$$

Averaging over initial-state spins ($2\times 2 = 4$) and colors ($N_c \times N_c = N_c^2$) and summing over all final-state spins and colors:

$$|\mathcal{M}_{q\bar{q}\to t\bar{t}}|^2 = \frac{g_s^4}{4N_c^2\,\hat{s}^2}\mathcal{C}_{q\bar{q}}\,\mathcal{D}^{\mu\nu\rho\sigma}_{q\bar{q}}\,g_{\mu\rho}g_{\nu\sigma}, \tag{52}$$

where $\mathcal{C}_{q\bar{q}}$ is the color factor and $\mathcal{D}^{\mu\nu\rho\sigma}_{q\bar{q}}$ is the product of Dirac traces.

Using the generator normalization $\mathrm{Tr}(T^aT^b) = T_F\delta^{ab} = \frac{1}{2}\delta^{ab}$ and Casimir relation:

$$\mathcal{C}_{q\bar{q}} = \sum_{a,b}\mathrm{Tr}(T^aT^b)\,\mathrm{Tr}(T^aT^b) = \left(\frac{1}{2}\delta^{ab}\right)\left(\frac{1}{2}\delta^{ab}\right) = \frac{1}{4}\delta^{ab}\delta^{ab} = \frac{N_c^2-1}{4}. \tag{53}$$

The leptonic/light-quark and heavy-quark tensor traces are:

$$L^{\mu\rho} = \mathrm{Tr}\left[\not{p}_2\gamma^\mu\not{p}_1\gamma^\rho\right] = 4\left(p_2^\mu p_1^\rho + p_1^\mu p_2^\rho - (p_1\cdot p_2)g^{\mu\rho}\right), \tag{54}$$

$$H_{\mu\rho} = \mathrm{Tr}\left[(\not{p}_3 + m_t)\gamma_\mu(\not{p}_4 - m_t)\gamma_\rho\right] = 4\left(p_{3\mu}p_{4\rho} + p_{4\mu}p_{3\rho} - (p_3\cdot p_4 + m_t^2)g_{\mu\rho}\right). \tag{55}$$

Contracting the two Lorentz tensors:

$$\begin{aligned}\mathcal{D}^{\mu\nu\rho\sigma}_{q\bar{q}}g_{\mu\rho}g_{\nu\sigma} = L^{\mu\rho}H_{\mu\rho} &= 16\left[2(p_1\cdot p_3)(p_2\cdot p_4) + 2(p_1\cdot p_4)(p_2\cdot p_3) + 2m_t^2(p_1\cdot p_2)\right]\\ &= 4\left[(m_t^2-\hat{t})^2 + (m_t^2-\hat{u})^2 + 2m_t^2\hat{s}\right]\\ &= 4\left[(\hat{t}-m_t^2)^2 + (\hat{u}-m_t^2)^2 + 2m_t^2\hat{s}\right].\end{aligned} \tag{56}$$

Combining the color factor and Dirac algebra:

$$|\mathcal{M}_{q\bar{q}\to t\bar{t}}|^2 = \frac{g_s^4}{4N_c^2\hat{s}^2}\left(\frac{N_c^2-1}{4}\right)\cdot 4\left[(\hat{t}-m_t^2)^2 + (\hat{u}-m_t^2)^2 + 2m_t^2\hat{s}\right], \tag{57}$$

$$= \frac{g_s^4(N_c^2-1)}{4N_c^2}\left[\frac{(\hat{t}-m_t^2)^2 + (\hat{u}-m_t^2)^2 + 2m_t^2\hat{s}}{\hat{s}^2}\right] \tag{58}$$

2.5.3 The Gluon-Gluon Fusion Channel

At leading order, gluon fusion receives contributions from three tree-level Feynman diagrams:

$$\mathcal{M}_{gg\to t\bar{t}} = \mathcal{M}_t + \mathcal{M}_u + \mathcal{M}_s. \tag{59}$$

1. **t-channel top exchange:**

$$
\begin{aligned}
i\mathcal{M}_t &= \bar{u}(p_3)(-ig_s\not{\epsilon}_1 T^a)\frac{i(\not{p}_3-\not{p}_1+m_t)}{(p_3-p_1)^2-m_t^2}(-ig_s\not{\epsilon}_2 T^b)v(p_4) \\
&= -ig_s^2(T^aT^b)_{kl}\frac{\bar{u}(p_3)\not{\epsilon}_1(\not{p}_3-\not{p}_1+m_t)\not{\epsilon}_2 v(p_4)}{\hat{t}-m_t^2}.
\end{aligned} \tag{60}
$$

2. **u-channel top exchange:**

$$
\begin{aligned}
i\mathcal{M}_u &= \bar{u}(p_3)(-ig_s\not{\epsilon}_2 T^b)\frac{i(\not{p}_3-\not{p}_2+m_t)}{(p_3-p_2)^2-m_t^2}(-ig_s\not{\epsilon}_1 T^a)v(p_4) \\
&= -ig_s^2(T^bT^a)_{kl}\frac{\bar{u}(p_3)\not{\epsilon}_2(\not{p}_3-\not{p}_2+m_t)\not{\epsilon}_1 v(p_4)}{\hat{u}-m_t^2}.
\end{aligned} \tag{61}
$$

3. **s-channel three-gluon vertex exchange:**

$$
\begin{aligned}
i\mathcal{M}_s &= \bar{u}(p_3)(-ig_s\gamma_\mu T^c_{kl})v(p_4)\left(\frac{-ig^{\mu\nu}}{\hat{s}}\right)g_s f^{abc}V_{\nu\alpha\beta}(p_1+p_2,-p_1,-p_2)\epsilon_1^\alpha\epsilon_2^\beta \\
&= -g_s^2 f^{abc}T^c_{kl}\frac{1}{\hat{s}}\left[\bar{u}(p_3)\gamma_\mu v(p_4)\right] \\
&\quad \left[g^{\mu\alpha}(p_1-p_2)^\beta + g^{\alpha\beta}(2p_2+p_1)^\mu - g^{\beta\mu}(2p_1+p_2)^\alpha\right]\epsilon_{1\alpha}\epsilon_{2\beta}.
\end{aligned} \tag{62}
$$

Using the Lie algebra relation $f^{abc}T^c = -i[T^a,T^b] = -i(T^aT^b - T^bT^a)$, the full amplitude can be decomposed into two gauge-invariant color structures:

$$
\mathcal{M}_{gg\to t\bar{t}} = g_s^2\left[(T^aT^b)_{kl}\mathcal{A} + (T^bT^a)_{kl}\mathcal{B}\right]. \tag{63}
$$

The color factors for the squared amplitude are:

$$
C_1 = \sum_{a,b}\mathrm{Tr}(T^aT^bT^bT^a) = C_F^2 N_c = \frac{(N_c^2-1)^2}{4N_c}, \tag{64}
$$

$$
C_2 = \sum_{a,b}\mathrm{Tr}(T^aT^bT^aT^b) = C_F\left(C_F - \frac{C_A}{2}\right)N_c = -\frac{N_c^2-1}{4N_c}. \tag{65}
$$

Averaging over initial gluon polarizations ($2\times 2 = 4$) and colors ($(N_c^2-1)^2 = 64$ for $N_c = 3$)and evaluating the complete Dirac traces and polarization sums (using $\sum \epsilon^\mu\epsilon^{*\nu} \to -g^{\mu\nu}$) yields:

$$
|\mathcal{M}_{gg\to t\bar{t}}|^2 = g_s^4\left[\frac{1}{2C_A}\frac{1}{\tau_t\tau_u} - \frac{C_A}{C_F C_A}\frac{\tau_t^2+\tau_u^2}{2\hat{s}^2}\right]\left[\frac{\tau_t^2+\tau_u^2+4m_t^2\hat{s}}{\hat{s}^2} - \frac{4m_t^4\hat{s}^2}{\tau_t^2\tau_u^2}\right] \tag{66}
$$

where $\tau_t \equiv \hat{t} - m_t^2$ and $\tau_u \equiv \hat{u} - m_t^2$.

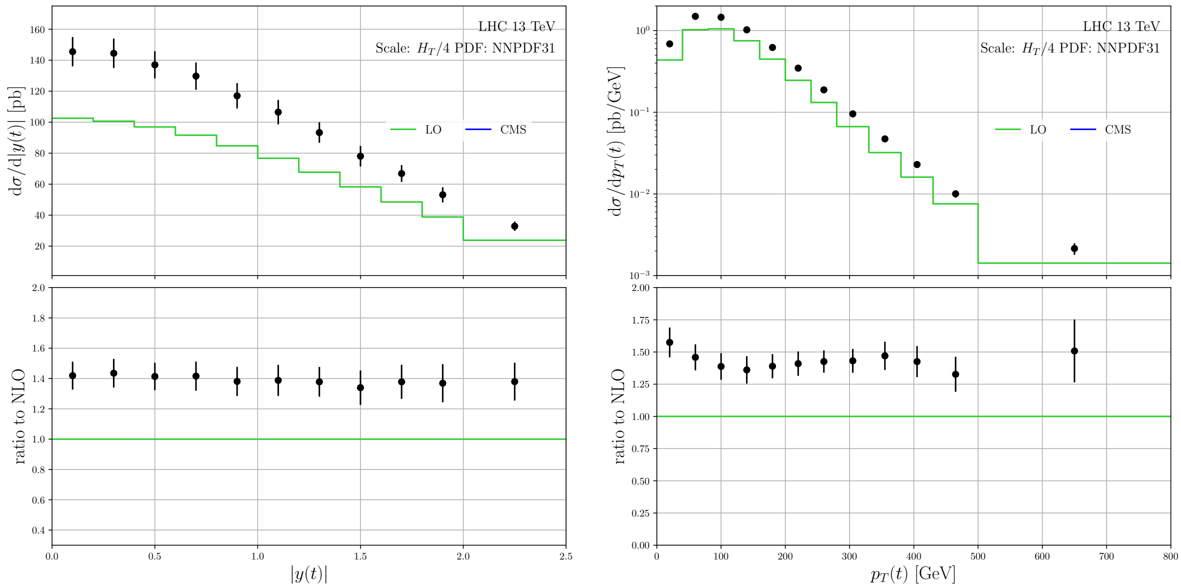

Figure 5: Leading order $pp \to t\bar{t}$ cross section compared to CMS data [6]

2.5.4 LHC predictions

We now have everything to predict partonic scattering cross sections for top-quark pair production at leading order. Since we don't have a quark or gluon collider, we are taking the LHC at 13 TeV proton-proton center-of-mass energy as an example. For now, consider the proton as a bunch of quarks and gluons with a probability of $f_i(x)$ determining their momentum fraction of the proton. These functions are the PDFs, and we will learn in Section 4 how they arise. In this simplified picture, the hadronic cross section for producing a top-quark pair reads:

$$\mathrm{d}\sigma_{pp\to t\bar{t}+X} = \sum_{a,b} \int_0^1 \mathrm{d}x_1 \mathrm{d}x_2 \, f_a(x_1)\, f_b(x_2)\, \mathrm{d}\hat{\sigma}_{ab}(x_1, x_2), \tag{67}$$

where $\mathrm{d}\hat{\sigma}_{ab}$ is our partonic cross section whose ingredients we computed above. Figure 5 shows the result of the (numerical) phase-space integration together with data from CMS [6].

We can observe that the prediction does not describe the data very well[3]. A general feature of QCD is that higher-order corrections play a major role and are important for describing data successfully.

[3]These plots suggest that it is mainly an issue in normalization; however, I injected already higher-order information through the scale choice $H_{T,4}$, which leads to a very good shape at LO; what this means we will discover in section 3.

3 Higher Orders

Going beyond tree-level computations requires some technical groundwork. First, we need to include loop diagrams that contain unconstrained integrations over loop momenta. The integrations will lead to divergences, which however can be treated with UV renormalization techniques. UV renormalization has profound consequences for QCD as it gives the possibility to describe asymptotic freedom.

Afterwards however we will face another type of divergence from the other end of the energy spectrum, namely infra-red divergencies that arise from unresolved particles. The treatment of infrared divergencies

3.1 Dimensional Regularisation and Renormalization

A simple example to see this is to consider the following diagram (view it as part of one, among many, one-loop diagrams that contribute to the first order corrections to $q\bar{q} \to t\bar{t}$) and look at its behaviour for large loop-momentum:

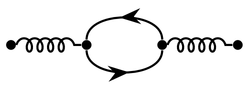

$$\sim \int \frac{\mathrm{d}^4 q}{(2\pi)^4} \frac{\mathrm{Tr}\left[\gamma^\mu(\not{q} + m)\gamma^\nu(\not{q} + \not{k} + m)\right]}{(q^2 - m^2)[(q+k)^2 - m^2]} \xrightarrow{|p|\to\infty} \int \mathrm{d}q \frac{1}{q} \tag{68}$$

This is a typical ultraviolet divergence present in many QFTs (QED and the EW theory have the same type of divergences). To handle these, we first need to introduce a regulator to make them finite. A simple option is to introduce a cut-off $|p| < \Lambda_{\mathrm{UV}}$ to restrict the integration, which, however, breaks Lorentz and gauge invariance. A more sophisticated option with better properties is dimensional regularisation, which analytically continues the theory into $d = 4 - 2\epsilon$ dimensions (this is what we will use in this lecture. In whatever way we regularize, we now have predictions that will depend not only on the theory parameters θ but also on a regularization parameter ϵ, $\mathcal{O}(\theta) \to \mathcal{O}(\theta, \epsilon)$. This means that if we try to extract parameters θ of the theory from data (for example through a fit of the predicted observables), these will also depend on ϵ, $\theta \to \theta(\epsilon)$. To have the theory make sense, we must demand that in the limit of $\epsilon \to 0$ the whole cycle leads to a finite limit and is independent of the regularisation method. While this is technically possible, it is challenging because it bakes in information about how the parameters have been extracted, i.e. which observables have been used.

The procedure of renormalization overcomes this shortcoming by absorbing the divergencies directly in the Lagrange parameters themselves and removing the divergencies from the predictions $\mathcal{O}^R(\theta, \epsilon) \xleftarrow{\epsilon\to 0} \mathcal{O}(\theta^R)$. One can show for some class of theories, the so-called renormalisable theories, this redefinition can be performed to all orders and is independent of the regularization scheme as well as the renormalization scheme (there are various options). Without diving into too much detail we will focus on renormalization in QCD which can be performed multiplicatively:

$$g_s^0 = \bar{\mu}^\epsilon Z_g g^R \,, \quad m_f^0 = Z_{m_f} m_f^R \,, \quad \Psi^0 = Z_\Psi^{1/2}\Psi^R \,, \quad A^0 = Z_A^{1/2} A^R \quad \xi^0 = Z_\xi \xi^R \,. \tag{69}$$

3.1.1 Dimensional Regularization

Dimensional regularization (DimReg or CDR) is the standard regularization scheme in Quantum Chromodynamics and gauge theories because it analytically continues spacetime to $D = 4 - 2\epsilon$ dimensions while preserving gauge invariance, Lorentz covariance, and unitarity. It regulates both ultraviolet (UV) and infrared (soft/collinear IR) singularities simultaneously as poles in $1/\epsilon$.

- **Loop Momentum Measure:** The 4-dimensional integration measure is replaced by:
$$\int \frac{d^4k}{(2\pi)^4} \longrightarrow \mu^{2\epsilon} \int \frac{d^Dk}{(2\pi)^D}, \qquad D = 4 - 2\epsilon, \tag{70}$$
where μ is an arbitrary 't Hooft renormalization scale introduced to keep the gauge coupling g_s dimensionless in D dimensions.

- **Metric and Dirac Algebra in D Dimensions:**
$$g^{\mu\nu} g_{\mu\nu} = D = 4 - 2\epsilon, \tag{71}$$
$$\gamma^\mu\gamma^\nu + \gamma^\nu\gamma^\mu = 2g^{\mu\nu}\mathbf{1}_{4\times 4}, \qquad \mathrm{Tr}[\mathbf{1}] = 4, \tag{72}$$
$$\gamma^\mu\gamma_\mu = D \cdot \mathbf{1} = (4 - 2\epsilon)\mathbf{1}, \tag{73}$$
$$\gamma^\mu \not{p} \gamma_\mu = (2 - D)\not{p} = (-2 + 2\epsilon)\not{p}, \tag{74}$$
$$\gamma^\mu\gamma^\nu\gamma_\mu = (2 - D)\gamma^\nu = (-2 + 2\epsilon)\gamma^\nu, \tag{75}$$
$$\gamma^\mu\gamma^\rho\gamma^\sigma\gamma_\mu = 4g^{\rho\sigma} - 2\epsilon\gamma^\rho\gamma^\sigma. \tag{76}$$

- **Scalar One-Loop Master Formula:** Using Feynman parameterization and Wick rotation, standard Euclidean loop integrals evaluate to:
$$\int \frac{d^Dk}{(2\pi)^D} \frac{1}{(k^2 - \Delta + i\varepsilon)^n} = \frac{(-1)^n i}{(4\pi)^{D/2}} \frac{\Gamma(n - D/2)}{\Gamma(n)} \left(\frac{1}{\Delta}\right)^{n - D/2} . \tag{77}$$
For the fundamental logarithmic divergence ($n = 2$):
$$\mu^{2\epsilon} \int \frac{d^Dk}{(2\pi)^D} \frac{1}{(k^2 - \Delta + i\varepsilon)^2} = \frac{i}{(4\pi)^2} \left(\frac{4\pi\mu^2}{\Delta}\right)^\epsilon \Gamma(\epsilon). \tag{78}$$

Expanding via $\Gamma(\epsilon) = \frac{1}{\epsilon} - \gamma_E + \mathcal{O}(\epsilon)$ and $A^\epsilon = 1 + \epsilon \ln A + \mathcal{O}(\epsilon^2)$:

$$\frac{i}{(4\pi)^2}\left[\frac{1}{\epsilon} - \gamma_E + \ln(4\pi) - \ln\left(\frac{\Delta}{\mu^2}\right) + \mathcal{O}(\epsilon)\right]. \tag{79}$$

- **Minimal Subtraction Schemes:**
  - **MS Scheme:** Absorbs only the pure pole term $\frac{1}{\epsilon}$ into the counterterms.
  - **$\overline{\text{MS}}$ Scheme:** Absorbs the universal combination $\frac{1}{\bar{\epsilon}} \equiv \frac{1}{\epsilon} - \gamma_E + \ln(4\pi)$, effectively setting the scale choice $\mu^2 \to \mu^2 \frac{e^{\gamma_E}}{4\pi}$.

Dimensional regularization is also applied to n-body phase-space measures $d\Phi_n$ to regulate soft and collinear singularities appearing in real radiation matrix elements. The formula in Equation 35 is extended to:

$$d\Phi_n(P) = \left(\frac{\mu^2 e^{\gamma_E}}{4\pi}\right)^{(n-1)\epsilon} (2\pi)^{4-2\epsilon}\delta^{(4-2\epsilon)}\left(P - \sum_{i=1}^{n} p_i\right)\prod_{i=1}^{n}\frac{d^{3-2\epsilon}\vec{p}_i}{(2\pi)^{3-2\epsilon}2E_i}, \tag{80}$$

The number of spin degrees of freedom for gluons also changes $n_g^{\text{spin}} = 2 \to n_g^{\text{spin}} = 2(1-\epsilon)$.

3.1.2 Ultraviolet Renormalization and the beta-function

Loop corrections in dimensional regularization ($D = 4 - 2\epsilon$) yield ultraviolet poles $1/\epsilon_{\text{UV}}$. In the $\overline{\text{MS}}$ scheme, the running strong coupling $\alpha_s(\mu_R^2) = \frac{g_s^2(\mu_R^2)}{4\pi}$ satisfies the renormalization group equation:

$$\mu_R^2 \frac{\partial \alpha_s}{\partial \mu_R^2} = \beta(\alpha_s) = -\alpha_s^2\left(b_0 + b_1\alpha_s + b_2\alpha_s^2 + \dots\right), \tag{81}$$

with the 1-loop and 2-loop coefficients:

$$b_0 = \frac{11C_A - 2n_f}{12\pi} = \frac{33 - 2n_f}{12\pi}, \tag{82}$$

$$b_1 = \frac{17C_A^2 - 5C_A n_f - 3C_F n_f}{24\pi^2} = \frac{153 - 19n_f}{24\pi^2}. \tag{83}$$

3.1.3 Asymptotic Freedom and the QCD Scale

For the physical Standard Model ($n_f \leq 6$), $b_0 > 0$. Solving the 1-loop RGE gives:

$$\alpha_s(Q^2) = \frac{\alpha_s(\mu_0^2)}{1 + b_0\alpha_s(\mu_0^2)\ln\left(\frac{Q^2}{\mu_0^2}\right)} \equiv \frac{1}{b_0 \ln\left(\frac{Q^2}{\Lambda_{\text{QCD}}^2}\right)}, \tag{84}$$

where $\Lambda_{\text{QCD}} \approx 200$–$300$ MeV is the non-perturbative scale parameter where the perturbative coupling diverges (Landau pole).

- **Asymptotic Freedom ($Q^2 \gg \Lambda^2_{\mathbf{QCD}}$):** $\alpha_s(Q^2) \to 0$. Quarks and gluons act as quasi-free particles; high-energy cross-sections are perturbatively calculable.

- **Confinement ($Q^2 \sim \Lambda^2_{\mathbf{QCD}}$):** $\alpha_s(Q^2) \sim \mathcal{O}(1)$. Non-perturbative dynamics dominate; isolated color charges cannot propagate as free asymptotic states.

World Average Reference Value: $\alpha_s(M_Z) = 0.1180 \pm 0.0009$.

3.2 Structure of NLO Calculations

The next-to-leading (NLO) coefficient reads:

$$d\hat{\sigma}^{(1)}_{ab} = d\hat{\sigma}^{\mathrm{R}}_{ab} + d\hat{\sigma}^{\mathrm{V}}_{ab} + d\hat{\sigma}^{\mathrm{C}}_{ab} \,, \tag{85}$$

where we have

$$\begin{aligned}
d\hat{\sigma}^{\mathrm{R}}_{ab} &= \frac{1}{2\hat{s}}\frac{1}{N_{ab}}\int \mathrm{d}\Phi_{Y+1}\, \langle \mathcal{M}^{(0)}_{ab\to Y+1} | \mathcal{M}^{(0)}_{ab\to Y+1}\rangle\, \mathcal{F}(\Phi_{Y+1}) \,, \\
d\hat{\sigma}^{\mathrm{V}}_{ab} &= \frac{1}{2\hat{s}}\frac{1}{N_{ab}}\int \mathrm{d}\Phi_{Y}\, 2\,\mathrm{Re}\, \langle \mathcal{M}^{(0)}_{ab\to Y} | \mathcal{M}^{(1)}_{ab\to Y}\rangle\, \mathcal{F}(\Phi_{Y}) \,, \\
d\hat{\sigma}^{\mathrm{C}}_{ab} &= \frac{\alpha_s}{2\pi}\frac{1}{\epsilon}\left(\frac{\mu_R^2}{\mu_F^2}\right)^{\epsilon} \sum_c \int_0^1 \mathrm{d}z \left[P^{(0)}_{ca}(z)\, \hat{\sigma}^{\mathrm{B}}_{cb}(zx_1, x_2) + P^{(0)}_{cb}(z)\, \hat{\sigma}^{\mathrm{B}}_{ac}(x_1, zx_2)\right] \,.
\end{aligned} \tag{86}$$

Crucially, the NLO QCD cross section involves two distinct phase spaces:

$$d\sigma^{\mathrm{NLO}} \ni \int_Y \mathrm{d}\sigma^{\mathrm{V}} + \int_Y \mathrm{d}\sigma^{\mathrm{R}}. \tag{87}$$

Using dimensional regularization ($D = 4 - 2\epsilon$):

- **Virtual corrections ($\mathrm{d}\sigma^{\mathbf{V}}$):** Contain loop integrals with ultraviolet poles (renormalized) and soft/collinear infrared poles ($\sim 1/\epsilon^2, 1/\epsilon$).

- **Real emissions ($\mathrm{d}\sigma^{\mathbf{R}}$):** Involve phase-space integration of tree-level $(m+1)$-body final states with unresolved soft and collinear radiation.

By the Kinoshita-Lee-Nauenberg (KLN) theorem, final-state infrared divergences cancel when integrated over degenerate states:

$$\mathrm{d}\sigma^{\mathrm{V}} + \int_1 \mathrm{d}\sigma^{\mathrm{R}} = \text{finite}. \tag{88}$$

Remaining initial-state collinear poles are factorized into the scale-dependent PDFs via the DGLAP evolution equations:

$$f_a(x, \mu_F^2) = f_a(x) - \frac{1}{\epsilon}\frac{\alpha_s}{2\pi}\sum_b \int_x^1 \frac{\mathrm{d}z}{z} P_{ab}(z) f_b(x/z). \tag{89}$$

3.3 An NLO example: electron-positron annihilation to hadrons

To explicitly see the cancellation of IR divergences, let's have a look at the example of electron-positron annihilation to hadrons. This process at next-to-leading order is described by the two partonic processes: $e^+(p_a) + e^-(p_b) \to \gamma^*(q) \to q(p_1) + \bar{q}(p_2)$ and $e^+(p_a) + e^-(p_b) \to \gamma^*(q) \to q(p_1) + \bar{q}(p_2) + (g(p_3))$. This process is the primary testing ground for perturbative QCD but is also simple enough to study on the blackboard in detail. The cross-section through single-photon exchange (lowest order in the electromagnetic coupling) factorizes into leptonic and hadronic tensors:

$$\sigma(e^+e^- \to X) = \frac{1}{2s}\frac{e^2}{s^2} L_{\mu\nu} H^{\mu\nu}. \tag{90}$$

The center-of-mass energy squared is given by

$$s = q^2 = (p_a + p_b)^2 \ , \tag{91}$$

and where the spin-averaged leptonic tensor for massless initial-state leptons is:

$$L_{\mu\nu} = \frac{1}{4} \operatorname{Tr}\left[\not{p}_b \gamma_\mu \not{p}_a \gamma_\nu\right] = p_{a\mu} p_{b\nu} + p_{a\nu} p_{b\mu} - g_{\mu\nu}(p_a \cdot p_b). \tag{92}$$

Contracting with the conserved electromagnetic current ($q^\mu H_{\mu\nu} = 0$), we have $H^{\mu\nu} = (q^\mu q^\nu - s g^{\mu\nu}) H(s)$, which yields:

$$L_{\mu\nu} H^{\mu\nu} = \frac{s}{3}\left(-g_{\mu\nu} H^{\mu\nu}\right). \tag{93}$$

Thus, the total cross section is proportional to the scalar trace $-g_{\mu\nu} H^{\mu\nu}$. All QCD corrections happen in $H^{\mu\nu}$ and thus we write:

$$H^{\mu\nu} = H^{(0)\,\mu\nu} + H^{(1)\,\mu\nu} + \mathcal{O}\big(\alpha_s^2\big) \tag{94}$$

where

$$H^{(0)\,\mu\nu} = \langle \mathcal{M}^{(0)\,\mu} | \mathcal{M}^{(0)\,\nu} \rangle \tag{95}$$

$$H^{(1)\,\mu\nu} = 2\,\mathrm{Re}(\langle \mathcal{M}^{(0)\,\mu} | \mathcal{M}^{(1)\,\nu} \rangle) \tag{96}$$

$$\tag{97}$$

3.3.1 Leading Order (LO) Born Cross-Section

To evaluate the total cross section in CDR, we need the two-body phase space in $d = 4 - 2\epsilon$ dimensions. The Lorentz-invariant n-body phase space in d dimensions is:

$$d\Phi_n(q; p_1, \ldots, p_n) = (2\pi)^d \delta^{(d)}\left(q - \sum_{i=1}^{n} p_i\right) \prod_{i=1}^{n} \frac{d^{d-1} p_i}{(2\pi)^{d-1} 2E_i}. \tag{98}$$

For $n = 2$ massless partons in the center-of-mass frame we can also calculate easily the total phase space volume:

$$\Phi_2 = \int d\Phi_2 = \frac{1}{8\pi}\left(\frac{4\pi}{s}\right)^{\epsilon}\frac{\Gamma(1-\epsilon)}{\Gamma(2-2\epsilon)}. \tag{99}$$

In $d = 4$ ($\epsilon = 0$), this reduces to the familiar $\Phi_2 = \frac{1}{8\pi}$. The Born amplitude for $\gamma^*(q) \to q(p_1)\bar{q}(p_2)$ is:

$$\mathcal{M}^{(0)\,\mu} = iee_q\bar{u}(p_1)\gamma^\mu v(p_2)\,\delta_{ij}, \tag{100}$$

where $i, j = 1, \ldots, N_c$ are color indices. Summing over colors and spins:

$$-g_{\mu\nu}H_0^{\mu\nu} = N_c e^2 e_q^2\,\mathrm{Tr}\left[\not{p}_1\gamma^\mu\not{p}_2\gamma_\mu\right] = 4(1-\epsilon)N_c e^2 e_q^2(2p_1\cdot p_2) = 4(1-\epsilon)N_c e^2 e_q^2 s. \tag{101}$$

Including the flux factor $\frac{1}{2s}$ and leptonic contraction we have in $d = 4$:

$$\sigma_0 \equiv \sigma^{\mathrm{LO}}(e^+e^- \to q\bar{q}) = \frac{4\pi\alpha_{\mathrm{em}}^2}{3s}N_c\sum_q e_q^2 = \sigma(e^+e^- \to \mu^+\mu^-) \times N_c\sum_q e_q^2. \tag{102}$$

3.3.2 Virtual Corrections

At NLO, the virtual corrections arise from the interference between the 1-loop and the tree-level amplitude. Working in $d = 4 - 2\epsilon$, the one-loop amplitude $\mathcal{M}^{(1)\,\mu}$ receives corrections from three diagrams: the vertex-correction and the quark self-energies. For massless on-shell quarks ($p^2 = 0$), the 1-loop self-energy integral $\Sigma(p)$ is scaleless:

$$\Sigma(\not{p}) \propto \int \frac{d^D k}{(2\pi)^D}\frac{1}{k^2(p-k)^2} \propto \frac{1}{\epsilon_{\mathrm{UV}}} - \frac{1}{\epsilon_{\mathrm{IR}}} = 0. \tag{103}$$

In dimensional regularization, scaleless integrals vanish because UV and IR divergences cancel algebraically. The wave-function renormalization constant in the on-shell scheme is $Z_2 = 1$. Consequently, the UV divergence is completely contained in the vertex correction and cancels against the bare electromagnetic current conservation ($Z_1 = Z_2$).

$$\mathcal{M}^{(1)\,\mu} = -ig_s^2\mu^{2\epsilon}(T^aT^a)_{ij}\int\frac{d^D k}{(2\pi)^D}\frac{\bar{u}(p_1)\gamma^\alpha(\not{p}_1 - \not{k})\gamma^\mu(-\not{p}_2 - \not{k})\gamma_\alpha v(p_2)}{[k^2 + i\epsilon][(p_1-k)^2 + i\epsilon][(p_2+k)^2 + i\epsilon]}. \tag{104}$$

Using the color Casimir $\sum_a (T^aT^a)_{ij} = C_F\delta_{ij}$ where $C_F = \frac{N_c^2-1}{2N_c} = \frac{4}{3}$, the Dirac numerator algebra simplifies in D dimensions ($\gamma^\alpha\not{a}\gamma_\alpha = -2(1-\epsilon)\not{a}$):

$$\mathcal{N}^\mu = -2(1-\epsilon)\not{k}\gamma^\mu\not{k} + 4(p_1\cdot p_2)\gamma^\mu - 4(p_1\cdot k)\gamma^\mu + 4(p_2\cdot k)\gamma^\mu - 4k^\mu(\not{p}_1 - \not{p}_2). \tag{105}$$

The terms with a single momentum k vanish due to the symmetry after integration over k^μ from $-\infty$ to ∞. The term with k^2 cancels against the denominator, and we receive a simple bubble integral.

Derivation: Massless Scalar Bubble Integral $B_0(p^2, 0, 0)$ We compute the dimensionally regularized scalar 2-point function in $D = 4 - 2\epsilon$ dimensions:

$$B_0(p^2, 0, 0) = \mu^{2\epsilon} \int \frac{\mathrm{d}^D k}{(2\pi)^D} \frac{1}{k^2 (k+p)^2}. \tag{106}$$

1. **Step 1: Feynman Parametrization.** Using the identity $\frac{1}{AB} = \int_0^1 \mathrm{d}x \frac{1}{[xA+(1-x)B]^2}$:

$$\frac{1}{k^2(k+p)^2} = \int_0^1 \mathrm{d}x \frac{1}{[x(k+p)^2 + (1-x)k^2]^2} = \int_0^1 \mathrm{d}x \frac{1}{[k^2 + 2x(k\cdot p) + xp^2]^2}. \tag{107}$$

2. **Step 2: Momentum Shift.** Shift the loop momentum $\ell^\mu = k^\mu + xp^\mu$. The denominator becomes:

$$\ell^2 - \Delta, \quad \text{with } \Delta = -x(1-x)p^2 - i\delta. \tag{108}$$

   Thus, the integral becomes:

$$B_0(p^2, 0, 0) = \mu^{2\epsilon} \int_0^1 \mathrm{d}x \int \frac{\mathrm{d}^D \ell}{(2\pi)^D} \frac{1}{[\ell^2 - \Delta]^2}. \tag{109}$$

3. **Step 3: Wick Rotation to Euclidean Space.** Rotating to Euclidean momentum $\ell^0 = i\ell_E^0$ such that $\ell^2 = -\ell_E^2$:

$$\int \frac{\mathrm{d}^D \ell}{(2\pi)^D} \frac{1}{[\ell^2 - \Delta]^2} = i \int \frac{\mathrm{d}^D \ell_E}{(2\pi)^D} \frac{1}{[\ell_E^2 + \Delta]^2} = \frac{i}{(4\pi)^{D/2}} \frac{\Gamma(2 - D/2)}{\Gamma(2)} \Delta^{D/2-2}. \tag{110}$$

4. **Step 4: Laurent Expansion in $\epsilon = (4-D)/2$.** Substituting $D = 4 - 2\epsilon$:

$$B_0(p^2, 0, 0) = \frac{i}{(4\pi)^2} (4\pi\mu^2)^\epsilon \Gamma(\epsilon) \int_0^1 \mathrm{d}x \left[-x(1-x)p^2 - i\delta\right]^{-\epsilon}. \tag{111}$$

   Expanding $\Gamma(\epsilon) = \frac{1}{\epsilon} - \gamma_E + \mathcal{O}(\epsilon)$ and $A^{-\epsilon} = 1 - \epsilon \ln A + \mathcal{O}(\epsilon^2)$:

$$\begin{aligned} &B_0(p^2, 0, 0) = \\ &\quad \frac{i}{(4\pi)^2} \left[\frac{1}{\epsilon} - \gamma_E + \ln(4\pi) + \ln\left(\frac{\mu^2}{-p^2 - i\delta}\right) - \int_0^1 \mathrm{d}x \ln[x(1-x)] + \mathcal{O}(\epsilon)\right]. \end{aligned} \tag{112}$$

   Since $\int_0^1 \mathrm{d}x \ln[x(1-x)] = -2$, we obtain the final result:

$$B_0(p^2, 0, 0) = \frac{i}{(4\pi)^2} \left[\frac{1}{\bar{\epsilon}} + \ln\left(\frac{\mu^2}{-p^2 - i\delta}\right) + 2 + \mathcal{O}(\epsilon)\right], \tag{113}$$

   where $\frac{1}{\bar{\epsilon}} \equiv \frac{1}{\epsilon} - \gamma_E + \ln(4\pi)$ is the standard $\overline{\text{MS}}$ pole.

For the remaining integrals, we can use the standard three-propagator Feynman parameter representation:

$$\frac{1}{ABC} = 2\int_0^1 dx \int_0^{1-x} dy \frac{1}{[xA + yB + (1-x-y)C]^3}, \tag{114}$$

with the shifted loop momentum $\ell = k - xp_1 + yp_2$, the denominator becomes $[\ell^2 - \Delta + i\epsilon]^3$ where $\Delta = -xys - i\epsilon$.

Integrating over ℓ using:

$$\int \frac{d^D\ell}{(2\pi)^D} \frac{1}{[\ell^2 - \Delta]^3} = \frac{-i}{(4\pi)^{D/2}} \frac{\Gamma(3 - D/2)}{2\,\Gamma(3)} \Delta^{D/2-3} = \frac{-i}{2(4\pi)^2}(4\pi)^{\epsilon}\frac{\Gamma(1+\epsilon)}{\Delta^{1+\epsilon}}, \tag{115}$$

we obtain the unrenormalized 1-loop vertex form factor:

$$F_1(s) = -\frac{\alpha_s C_F}{2\pi} \frac{\Gamma(1+\epsilon)\Gamma^2(1-\epsilon)}{\Gamma(1-2\epsilon)} \left(\frac{4\pi\mu^2}{-s - i\epsilon}\right)^{\epsilon} \left[\frac{1}{\epsilon^2} + \frac{3}{2\epsilon} + 4 + \mathcal{O}(\epsilon)\right]. \tag{116}$$

Putting everything together (the algebra is left to the reader `;-)`), the virtual contribution to the cross section is:

$$\sigma^{\mathrm{V}} = \sigma_0 \frac{\alpha_s C_F}{2\pi} \left(\frac{4\pi\mu^2}{s}\right)^{\epsilon} \frac{\Gamma(1-\epsilon)^2\Gamma(1+\epsilon)}{\Gamma(1-2\epsilon)} \left[-\frac{2}{\epsilon^2} - \frac{3}{\epsilon} - 8 + \frac{7\pi^2}{6} + \mathcal{O}(\epsilon)\right]. \tag{117}$$

The virtual contribution contains:

- A double pole $-2/\epsilon^2$ corresponding to the soft-and-collinear region.
- A single pole $-3/\epsilon$ corresponding to the hard-collinear collinear region.

3.3.3 Real Emission Corrections

For $e^+e^- \to q(p_1) + \bar{q}(p_2) + g(p_3)$, let $x_i = \frac{2p_i \cdot q}{s}$ be the energy fractions in the CM frame $(x_1 + x_2 + x_3 = 2)$. The invariant masses of pairs are:

$$s_{12} = s(1 - x_3), \quad s_{13} = s(1 - x_2), \quad s_{23} = s(1 - x_1). \tag{118}$$

The 3-body phase space in $D = 4 - 2\epsilon$ dimensions parameterized by x_1, x_2 is:

$$d\Phi_3 = \frac{s^{1-2\epsilon}}{32(2\pi)^3}\left(\frac{4\pi}{s}\right)^{2\epsilon} \frac{1}{\Gamma(2-2\epsilon)}(1-x_1)^{-\epsilon}(1-x_2)^{-\epsilon}(x_1+x_2-1)^{-\epsilon}dx_1dx_2. \tag{119}$$

The physical Dalitz region is defined by:

$$0 \le x_1, x_2 \le 1, \quad x_1 + x_2 \ge 1. \tag{120}$$

The matrix element, summed over all polarizations and colors for $\gamma^* \to q\bar{q}g$:

$$|\mathcal{M}_R|^2 = 4(1-\epsilon)g_s^2\mu^{2\epsilon}e^2e_q^2N_cC_F\left[\frac{x_1^2 + x_2^2 - \epsilon(2 - x_1 - x_2)^2}{(1-x_1)(1-x_2)}\right]. \tag{121}$$

Combining the phase space and matrix element:

$$\begin{aligned}\sigma^{\text{real}} =& \sigma_0 \frac{\alpha_s C_F}{2\pi} \left(\frac{4\pi\mu^2}{s}\right)^{\epsilon} \frac{\Gamma(1-\epsilon)}{\Gamma(2-3\epsilon)} \\ & \int_0^1 dx_1 \int_{1-x_1}^1 dx_2 \frac{x_1^2 + x_2^2 - \epsilon(2 - x_1 - x_2)^2}{(1-x_1)^{1+\epsilon}(1-x_2)^{1+\epsilon}(x_1+x_2-1)^{\epsilon}}.\end{aligned} \tag{122}$$

Explicit Integration of the real cross-section To evaluate the singular integral, let $x_2 = 1 - v(1 - x_1)$ where $v \in [0, 1]$:

$$\int_0^1 dx_1 (1-x_1)^{-1-2\epsilon} \int_0^1 dv\, v^{-1-\epsilon}(1-v)^{-\epsilon} \left[x_1^2 + (1 - v(1-x_1))^2 - \epsilon(1-x_1)^2(1+v)^2\right]. \tag{123}$$

Using the Euler Beta function $B(a, b) = \int_0^1 dt\, t^{a-1}(1-t)^{b-1} = \frac{\Gamma(a)\Gamma(b)}{\Gamma(a+b)}$:

$$\sigma^{\text{real}} = \sigma_0 \frac{\alpha_s C_F}{2\pi} \left(\frac{4\pi\mu^2}{s}\right)^{\epsilon} \frac{\Gamma(1-\epsilon)^2\Gamma(1+\epsilon)}{\Gamma(1-2\epsilon)} \left[\frac{2}{\epsilon^2} + \frac{3}{\epsilon} + \frac{19}{2} - \frac{7\pi^2}{6} + \mathcal{O}(\epsilon)\right]. \tag{124}$$

3.3.4 Total NLO Cross-Section & The KLN Cancellation

Combining the virtual and real corrections, we observe an exact, algebraic cancellation of all double ($1/\epsilon^2$) and single ($1/\epsilon$) infrared poles:

$$\begin{aligned}\sigma^{\text{NLO}} &= \sigma_0 + \sigma^{\text{virtual}} + \sigma^{\text{real}} \\ &= \sigma_0 \left\{1 + \frac{\alpha_s C_F}{2\pi} \left[\left(-\frac{2}{\epsilon^2} - \frac{3}{\epsilon} - 8 + \frac{7\pi^2}{6}\right) + \left(\frac{2}{\epsilon^2} + \frac{3}{\epsilon} + \frac{19}{2} - \frac{7\pi^2}{6}\right)\right]\right\} \\ &= \sigma_0 \left\{1 + \frac{\alpha_s C_F}{2\pi}\left(\frac{19}{2} - 8\right)\right\} \\ &= \sigma_0 \left(1 + \frac{3C_F}{4\pi}\alpha_s\right).\end{aligned} \tag{125}$$

Substituting the color Casimir $C_F = \frac{4}{3}$:

$$\sigma^{\text{NLO}}(e^+e^- \to \text{hadrons}) = \sigma_0 \left(1 + \frac{\alpha_s(s)}{\pi}\right). \tag{126}$$

3.4 Universal Factorization in the Singular Limits

In fixed-order perturbation theory, multi-parton amplitudes develop severe infrared (IR) divergences when additional emitted partons are soft (energy $E \to 0$) or collinear (angle $\theta \to 0$) relative to the emitting colored parton. Far from being merely computational hurdles, these singular limits have a universal, process-independent factorization structure that underpins subtraction methods, all-order resummation and the Monte Carlo parton shower paradigm.

3.4.1 The Soft Limit and Eikonal Currents

Consider the emission of a soft gluon with momentum k^μ ($k^0 = \omega \ll E_i$) from an outgoing on-shell quark line with momentum p^μ ($p^2 = m^2$). The uncontracted Feynman amplitude for this emission is given by:

$$\mathcal{M}_{n+1} \sim \bar{u}(p)\,(-ig_s T^a \not{\epsilon}^*(k))\,\frac{i(\not{p} + \not{k} + m)}{(p+k)^2 - m^2}\,\Gamma, \tag{127}$$

where Γ represents the remainder of the hard scattering process. Using the Dirac equation $\bar{u}(p)(\not{p} - m) = 0$ and the on-shell condition $k^2 = 0$, the propagator denominator reduces to $(p+k)^2 - m^2 = 2p \cdot k$. The numerator becomes:

$$\bar{u}(p)\not{\epsilon}^*(\not{p} + \not{k} + m) = \bar{u}(p)\left(2p \cdot \epsilon^* - (\not{p} - m)\not{\epsilon}^* + \not{\epsilon}^*\not{k}\right) \approx 2(p \cdot \epsilon^*)\,\bar{u}(p), \tag{128}$$

where the non-commuting term $\not{\epsilon}^*\not{k} \sim \mathcal{O}(\omega)$ is neglected relative to $p \cdot \epsilon^* \sim \mathcal{O}(E_p)$. Hence, the emission amplitude simplifies to the classical Eikonal approximation:

$$\mathcal{M}_{n+1} \approx g_s T^a \left(\frac{p \cdot \epsilon^*(k)}{p \cdot k}\right) \mathcal{M}_n. \tag{129}$$

Notice that the soft gluon emission is entirely spin-independent; the soft gluon couples exclusively to the classical color current associated with the 4-velocity of the emitting particle.

For an overall color-singlet dipole system (e.g., $e^+e^- \to q(p_1) + \bar{q}(p_2) + g(k)$), the amplitude is the sum of the radiation from both legs:

$$\mathcal{M}_{q\bar{q}g} \approx g_s T^a \left(\frac{p_1 \cdot \epsilon^*}{p_1 \cdot k} - \frac{p_2 \cdot \epsilon^*}{p_2 \cdot k}\right) \mathcal{M}_{q\bar{q}}. \tag{130}$$

Squaring the amplitude and summing over physical gluon polarizations $\sum_{\text{pol}} \epsilon^\mu \epsilon^{*\nu} = -g^{\mu\nu}$ (in a physical gauge):

$$|\mathcal{M}_{q\bar{q}g}|^2 \simeq g_s^2 C_F \left(-\frac{p_1}{p_1 \cdot k} + \frac{p_2}{p_2 \cdot k}\right)^2 |\mathcal{M}_{q\bar{q}}|^2 = g_s^2 C_F \left[\frac{2p_1 \cdot p_2}{(p_1 \cdot k)(p_2 \cdot k)}\right] |\mathcal{M}_{q\bar{q}}|^2. \tag{131}$$

The single-gluon Lorentz-invariant phase space is:

$$d\Phi_g = \frac{d^3\vec{k}}{(2\pi)^3 2\omega} = \frac{\omega\, d\omega\, d\cos\theta\, d\phi}{2(2\pi)^3}. \tag{132}$$

Thus, the soft emission probability factorizes into:

$$d\mathcal{P}_{\text{soft}} = \frac{\alpha_s C_F}{\pi} \frac{d\omega}{\omega} \frac{d\cos\theta\, d\phi}{2\pi} \left[\frac{1 - \cos\theta_{12}}{(1 - \cos\theta_{1k})(1 - \cos\theta_{2k})}\right]. \tag{133}$$

3.4.2 The Collinear Limit and Splitting Kernels

When two partons b and c become collinear ($\theta_{bc} \to 0$, virtuality $t = (p_b + p_c)^2 \to 0$), the matrix element factorizes into the n-parton Born matrix element and the universal Altarelli-Parisi splitting functions:

$$d\sigma_{n+1} \xrightarrow{\text{collinear}} d\sigma_n \times \frac{\alpha_s}{2\pi}\frac{dt}{t}\, dz\, \frac{d\phi}{2\pi}\, \hat{P}_{a\to bc}(z), \tag{134}$$

where z is the longitudinal energy fraction carried away by daughter parton b, and $(1-z)$ is carried by daughter parton c. The unregularized (real-emission) splitting kernels are:

$$\hat{P}_{q\to qg}(z) = C_F \left[\frac{1+z^2}{1-z}\right], \tag{135}$$

$$\hat{P}_{g\to q\bar{q}}(z) = T_F \left[z^2 + (1-z)^2\right], \tag{136}$$

$$\hat{P}_{g\to gg}(z) = 2C_A \left[\frac{z}{1-z} + \frac{1-z}{z} + z(1-z)\right]. \tag{137}$$

In the overlapping soft-collinear limit ($z \to 1$ and $t \to 0$), we recover the double-logarithmic structure:

$$\frac{dt}{t} dz \hat{P}_{q\to qg}(z) \approx 2C_F \frac{dt}{t}\frac{dz}{1-z} \sim 2C_F \frac{dk_\perp}{k_\perp}\frac{d\omega}{\omega}. \tag{138}$$

3.5 NLO Subtraction Methods

For exclusive observables (e.g., differential jet cross-sections with kinematic cuts), analytical phase-space integration is impossible. To compute $\sigma^{\text{NLO}}_{\text{obs}}$ numerically via Monte Carlo, one must isolate and cancel IR singularities at the integrand level using subtraction methods.

The general idea is as follows. Let J_n and J_{n+1} be the measurement functions defining the observable for n and $n+1$ partons. The general NLO cross section is written as:

$$\sigma^{\text{NLO}} = \int d\Phi_{n+1} \left[d\sigma^R J_{n+1} - d\sigma^S J_n\right] + \int d\Phi_n \left[d\sigma^V + \int_1 d\sigma^S\right] J_n, \tag{139}$$

where $d\sigma^S$ is a local counterterm that matches the pointwise singular behavior of the real cross-section $d\sigma^R$ in all soft and collinear limits:

$$\lim_{\text{soft/collinear}} \left(d\sigma^R - d\sigma^S\right) = 0. \tag{140}$$

Consequently:

1. The first bracket $[d\sigma^R J_{n+1} - d\sigma^S J_n]$ is strictly finite in 4 dimensions ($\epsilon = 0$) and can be integrated numerically.

2. The integrated subtraction term $\int_1 d\sigma^S$ is integrated analytically in D dimensions over the 1-parton unresolved phase space, yielding explicit poles in $1/\epsilon^2$ and $1/\epsilon$ that cancel the virtual poles in $d\sigma^V$.

Schemes at NLO:

- Catani-Seymour (CS) Dipole Subtraction [7]
- Frixione-Kunszt-Signer (FKS) Subtraction [8]

3.6 Beyond NLO

3.6.1 Structure of the cross section

An NNLO calculation for a $2 \to 2$ multi-boson process ($pp \to V_1 V_2$) receives contributions from three distinct phase-space sectors:

$$\sigma^{\mathrm{NNLO}} = \int_m \mathrm{d}\sigma^{\mathrm{VV}} + \int_{m+1} \mathrm{d}\sigma^{\mathrm{RV}} + \int_{m+2} \mathrm{d}\sigma^{\mathrm{RR}}, \tag{141}$$

where:

- **Double-Virtual** ($\mathrm{d}\sigma^{\mathrm{VV}}$): Involves 2-loop amplitudes interfering with Born plus squared 1-loop amplitudes:

$$\mathrm{d}\sigma^{\mathrm{VV}} \propto 2\,\mathrm{Re}\langle \mathcal{M}_0 | \mathcal{M}_2 \rangle] + |\mathcal{M}_1|^2. \tag{142}$$

  Contains infrared and ultraviolet poles up to ϵ^{-4} in dimensional regularization ($D = 4 - 2\epsilon$).

- **Real-Virtual** ($\mathrm{d}\sigma^{\mathrm{RV}}$): 1-loop corrections to single-real emission matrix elements ($q\bar{q} \to V_1 V_2 + g$). Features overlapping infrared singularities up to ϵ^{-3}.

- **Double-Real** ($\mathrm{d}\sigma^{\mathrm{RR}}$): Tree-level amplitudes with two unresolved partonic emissions ($q\bar{q} \to V_1 V_2 + gg$, $qg \to V_1 V_2 + qg$, etc.), yielding singular phase-space integrations up to ϵ^{-4}.

3.6.2 Modern NNLO Subtraction Formalisms

Because of overlapping and nested double-unresolved infrared limits, isolating singularities requires advanced subtraction methods:

- q_T**-Subtraction (Slicing):** Exploits the transverse momentum q_T of the diboson system. Above a slicing parameter $q_{T,\text{cut}}$, the process corresponds to an NLO calculation of Y + jet. In the limit $q_T \to 0$, the singular cross section is predicted analytically via Soft-Collinear Effective Theory (SCET):

$$\mathrm{d}\sigma^{\mathrm{NNLO}} = \mathcal{H}^{\mathrm{NNLO}} \otimes \mathrm{d}\sigma^{\mathrm{Born}} + \left[\mathrm{d}\sigma^{\mathrm{NLO}}_{Y+\mathrm{jet}} - \mathrm{d}\sigma^{\mathrm{CT}}\right]_{q_T > q_{T\mathrm{cut}}}. \tag{143}$$

- N**-Jettiness Subtraction (**$\mathcal{T}_N$**):** Slicing technique based on global N-jettiness event shapes.

- **Antenna Subtraction:** Fully local subtraction formalisms based on antenna functions or inclusive kinematic projections.

- **Sector-improved residue subtraction:** also a fully local scheme similar to FKS. Depending on implementation with numerical[9] or analytical integration of subtraction terms.

- **Projection-to-Born**

3.7 Infrared and Collinear (IRC) Safety

An observable $\mathcal{O}$ defined for an n-parton state $\mathcal{O}_n(p_1, \dots, p_n)$ is **Infrared and Collinear Safe** if it is invariant under the emission of an infinitesimally soft parton or a collinear splitting:

$$\lim_{p_{n+1} \to 0} \mathcal{O}_{n+1}(p_1, \dots, p_n, p_{n+1}) = \mathcal{O}_n(p_1, \dots, p_n) \quad \text{(Soft Safety)}, \tag{144}$$

$$\lim_{p_i \| p_j} \mathcal{O}_{n+1}(\dots, p_i, p_j, \dots) = \mathcal{O}_n(\dots, p_i + p_j, \dots) \quad \text{(Collinear Safety)}. \tag{145}$$

Examples:

- *IRC Safe:* Total cross-sections, Jet rates defined via sequential recombination algorithms, Thrust $T = \max_{\vec{n}} \frac{\sum_i |\vec{p}_i \cdot \vec{n}|}{\sum_i |\vec{p}_i|}$.

- *IRC Unsafe:* Total hadron multiplicity, the energy of the single hardest hadron in a jet. Naive jet flavor definitions.

4 Hadron Structure, Deep Inelastic Scattering, and PDFs

In lepton-induced processes such as $e^+e^- \to$ hadrons, the initial state is purely leptonic and color-singlet, confining all non-Abelian gauge dynamics strictly to the final state. By contrast, in lepton-hadron ($e^-P \to e^-X$) and hadron-hadron ($pp \to X$) collisions, colored bound states enter the initial state. This introduces three fundamental field-theoretic and practical challenges:

1. **Non-Perturbative Confinement:** Quarks and gluons inside a proton are bound by strong-coupling dynamics characterized by the non-perturbative scale $\Lambda_{\rm QCD} \approx$ 200-300 MeV. Free partonic asymptotic states do not exist.

2. **Initial-State Collinear Singularities:** When an incoming colored parton radiates a collinear gluon prior to hard scattering, the resulting collinear divergence cannot be cancelled by final-state summing. The Kinoshita-Lee-Nauenberg (KLN) theorem does not apply because the initial state is fixed rather than summed over degenerate configurations.

3. **Beam Remnants and Soft Activity:** The unscattered components of colliding hadrons carry net color charge, generating initial-state radiation (ISR), soft multi-parton interactions (MPI), and underlying event (UE) contamination.

4.1 Deep Inelastic Scattering

The internal structure of hadrons is probed systematically via lepton-nucleon Deep Inelastic Scattering:

$$e^-(k) + P(P) \longrightarrow e^-(k') + X(P_X). \tag{146}$$

The interaction proceeds through the exchange of a spacelike virtual photon with four-momentum:

$$q^\mu = k^\mu - k'^\mu, \quad Q^2 \equiv -q^2 = 4E_k E_{k'} \sin^2\left(\frac{\theta}{2}\right) > 0. \tag{147}$$

The hard virtuality Q^2 sets the transverse spatial resolution $\Delta r_\perp \sim 1/Q$ probing the nucleon.

Lorentz-Invariant Kinematics

- **Bjorken Scaling Variable:**

$$x \equiv x_{\rm Bj} = \frac{Q^2}{2P\cdot q} \in [0,1]. \tag{148}$$

In the infinite-momentum frame, x represents the fraction of the nucleon's longitudinal momentum carried by the struck parton.

- **Inelasticity:**

$$y \equiv \frac{P \cdot q}{P \cdot k} \in [0, 1], \tag{149}$$

measuring the fractional energy loss of the electron in the target rest frame ($y = (E_k - E_{k'})/E_k$).

- **Center-of-Mass Invariant:**

$$s = (k + P)^2 \approx 2P \cdot k \implies Q^2 = xys. \tag{150}$$

- **Hadronic Invariant Mass Squared:**

$$W^2 = (P + q)^2 = M^2 + Q^2 \left(\frac{1 - x}{x} \right) \geq M^2. \tag{151}$$

Hadronic Tensor Decomposition The unpolarized differential cross section factorizes into leptonic and hadronic tensors:

$$d\sigma = \frac{1}{4ME} \frac{d^3k'}{(2\pi)^3 2E_{k'}} \frac{e^4}{Q^4} L^{\mu\nu} W_{\mu\nu}. \tag{152}$$

The spin-averaged leptonic tensor for massless Dirac electrons is:

$$L_{\mu\nu} = \frac{1}{2} \operatorname{Tr} \left[\not{k}' \gamma_\mu \not{k} \gamma_\nu \right] = 2 \left(k_\mu k'_\nu + k'_\mu k_\nu - g_{\mu\nu} (k \cdot k') \right). \tag{153}$$

Lorentz covariance, parity conservation, and electromagnetic current conservation ($q^\mu W_{\mu\nu} = 0$) restrict the parameterization of $W_{\mu\nu}$ to two independent structure functions:

$$W_{\mu\nu}(P, q) = \left(-g_{\mu\nu} + \frac{q_\mu q_\nu}{q^2} \right) W_1(x, Q^2) + \left(P_\mu - q_\mu \frac{P \cdot q}{q^2} \right) \left(P_\nu - q_\nu \frac{P \cdot q}{q^2} \right) \frac{W_2(x, Q^2)}{P \cdot q}. \tag{154}$$

Defining the dimensionless structure functions $F_1(x, Q^2) \equiv W_1(x, Q^2)$ and $F_2(x, Q^2) \equiv \frac{P \cdot q}{M^2} W_2(x, Q^2)$:

$$\frac{d^2\sigma}{dx\, dy} = \frac{4\pi\alpha_{\text{em}}^2 s}{Q^4} \left[y^2 x F_1(x, Q^2) + (1 - y) F_2(x, Q^2) - \frac{M^2 xy}{s} F_2(x, Q^2) \right]. \tag{155}$$

If we allow for weak interactions more structure functions would appear.

4.2 The Naive Quark-Parton Model and Bjorken Scaling

In the Bjorken limit ($Q^2, P\cdot q \to \infty$ with x fixed), the lifetime of the virtual photon probe $\tau \sim 1/Q$ is much shorter than the characteristic timescale of internal non-perturbative interactions $\tau_{\text{int}} \sim 1/\Lambda_{\text{QCD}}$. The virtual photon scatters incoherently off quasi-free, collinear quarks carrying momentum $p^\mu = \xi P^\mu$:

$$(p+q)^2 = m_q^2 \approx 0 \implies (\xi P + q)^2 \approx 2\xi P\cdot q - Q^2 = 0 \implies \xi = x_{\text{Bj}}. \tag{156}$$

Interpreting quarks as spin-1/2 Dirac fermions we know that they couple only to transverse virtual photons in the collinear limit. Hence, the longitudinal structure function F_L vanishes:

$$F_L(x) \equiv F_2(x) - 2xF_1(x) = 0 \implies F_2(x) = 2xF_1(x) \quad (\textbf{Callan-Gross Relation}). \tag{157}$$

For spin-0 partons, $F_1(x) = 0$, establishing the Callan-Gross relation as direct experimental evidence that quarks carry spin 1/2.

Parton Interpretation We can redo the calculus above for the case of a quark scattering with an electron. Let assume that the quarks momentum is $p = \omega P$, where P is the momentum we had for the proton and $\omega \in [0,1]$. We can calculate now the matrix element

$$\frac{1}{4}\sum_{\text{pol}} |\mathcal{M}|^2 = \frac{e^4 e_f^2}{Q^4} L^{\mu\nu} Q_{\mu\nu}\ , \quad Q^{\mu\nu} = p^\mu p'^\nu + p^\nu p'^\mu - g^{\mu\nu}(p\cdot p') \tag{158}$$

and parameterize the phase space explicitly

$$\mathrm{d}\Phi_2 = \frac{\mathrm{d}^3k'}{(2\pi)^3 2E'} \frac{\mathrm{d}^4p'}{(2\pi)^3} \delta(p'^2)(2\pi)^4\delta^4(k+p-k'-p') = \frac{\mathrm{d}\phi}{(4\pi)^2}\mathrm{d}x\mathrm{d}y\delta(\omega - x)\ . \tag{159}$$

We find then for the cross section

$$\frac{\mathrm{d}^2\sigma}{\mathrm{d}x\mathrm{d}y} = \frac{4\pi\alpha}{yQ^4}\left[1+(1-y)^2\right]\frac{1}{2}e_f^2\delta(\omega - x)\ . \tag{160}$$

Here we see that the longitudinal term proportional to $(1-y)/x$ does not even appear (we showed effectively the Callan Gross relation for quarks).

Naive quark model If, at leading order, we interpret the $f_i(\omega)$ as the probability to find a quark of flavor i with momentum fraction ω, then we can write the hadronic object F_2.

$$F_2(x) = \sum_i \int \mathrm{d}\omega f_i(\omega) x e_{f_i}^2 \delta(x-\omega) = \sum_i e_{f_i}^2 f_i(x) x \tag{161}$$

The $f_i(x)$ are called the Parton Distribution Function (PDF), representing the probability density of finding a parton of flavor i carrying momentum fraction x. Proton quantum numbers impose valence sum rules:

$$\int_0^1 \mathrm{d}x\,[u(x) - \bar{u}(x)] = 2, \tag{162}$$

$$\int_0^1 \mathrm{d}x\,[d(x) - \bar{d}(x)] = 1, \tag{163}$$

$$\int_0^1 \mathrm{d}x\,[s(x) - \bar{s}(x)] = 0. \tag{164}$$

4.3 Radiative QCD Corrections

At $\mathcal{O}(\alpha_s)$, real gluon emission from the struck incoming quark ($\gamma^* + q \to q + g$) introduces scale violations. Parameterizing the kinematics with $p = \xi P$ and longitudinal splitting fraction z:

$$z = \frac{x}{\xi} = \frac{Q^2}{2p \cdot q} \in [x, 1]. \tag{165}$$

Evaluating the partonic structure function $\hat{F}_{2,q}$ in dimensional regularization ($D = 4-2\epsilon$):

$$\hat{F}_{2,q}\left(z, \frac{Q^2}{\mu^2}\right) = e_q^2\, z \left\{\delta(1-z) + \frac{\alpha_s}{2\pi} P_{qq}(z) \left[-\frac{1}{\epsilon_{\mathrm{IR}}} \left(\frac{4\pi\mu^2}{Q^2}\right)^{\epsilon} \frac{\Gamma(1-\epsilon)\Gamma^2(1+\epsilon)}{\Gamma(1+2\epsilon)}\right] + C_q(z)\right\}. \tag{166}$$

The factor $P_{qq}(z)$ is the Altarelli-Parisi quark-to-quark splitting kernel:

$$P_{qq}(z) = C_F \left[\frac{1+z^2}{(1-z)_+} + \frac{3}{2}\delta(1-z)\right]. \tag{167}$$

The pole $-1/\epsilon_{\mathrm{IR}}$ corresponds to collinear gluon emission parallel to the incoming quark. Unlike final-state emissions, this singularity cannot cancel against virtual corrections because the initial state is fixed to a single incoming parton flavor and momentum.

The Collinear Factorization Theorem The systematic treatment of initial-state collinear singularities is governed by the **Collinear Factorization Theorem** (proven by Collins, Soper, and Sterman).

Mass Factorization in the $\overline{\mathrm{MS}}$ Scheme The bare PDF $f_i^{(0)}(\xi)$ is related to the renormalized PDF $f_i(x, \mu_F^2)$ by subtracting the collinear pole:

$$f_i(x, \mu_F^2) = f_i^{(0)}(x) - \frac{1}{\epsilon_{\mathrm{IR}}} \left(\frac{4\pi\mu^2}{\mu_F^2}\right)^{\epsilon} \frac{\Gamma(1+\epsilon)}{16\pi^2} \sum_j \int_x^1 \frac{dz}{z} P_{ij}(z) f_j\left(\frac{x}{z}\right). \tag{168}$$

The physical structure function $F_2(x,Q^2)$ factorizes into a convolution:

$$F_2(x,Q^2) = \sum_{i=q,\bar{q},g} \int_x^1 \frac{dz}{z} C_{2,i}\left(\frac{x}{z}, \frac{Q^2}{\mu_F^2}, \alpha_s(\mu_R^2)\right) f_i(z,\mu_F^2) + \mathcal{O}\left(\frac{\Lambda_{\text{QCD}}^2}{Q^2}\right), \tag{169}$$

where:

- $C_{2,i}$: Process-dependent, infrared-finite coefficient functions calculable in perturbation theory in powers of $\alpha_s(\mu_R^2)$.
- $f_i(z,\mu_F^2)$: Process-independent, universal PDFs.
- $\mathcal{O}(\Lambda_{\text{QCD}}^2/Q^2)$: Non-perturbative higher-twist corrections.

4.4 The DGLAP Evolution Equations

Because the bare distribution $f_i^{(0)}(x)$ is independent of the arbitrary factorization scale μ_F, the condition $df_i^{(0)}/d\ln\mu_F^2 = 0$ leads directly to the **Dokshitzer-Gribov-Lipatov-Altarelli-Parisi (DGLAP)** evolution equations:

$$\frac{\partial f_i(x,\mu_F^2)}{\partial \ln\mu_F^2} = \frac{\alpha_s(\mu_F^2)}{2\pi} \sum_j \int_x^1 \frac{dz}{z} P_{ij}(z)\, f_j\left(\frac{x}{z}, \mu_F^2\right). \tag{170}$$

Singlet and Non-Singlet Decomposition To solve the coupled system of $2n_f + 1$ equations, distributions are decomposed into non-singlet and singlet combinations:

1. **Non-Singlet Combinations ($q_{\mathbf{NS}} = q_i - q_j$ or $q_i - \bar{q}_i$):**

   Decouples completely from the gluon distribution, conserving valence quark numbers:

$$\frac{\partial q_{\text{NS}}(x,\mu_F^2)}{\partial \ln\mu_F^2} = \frac{\alpha_s(\mu_F^2)}{2\pi} \int_x^1 \frac{dz}{z} P_{qq}(z)\, q_{\text{NS}}\left(\frac{x}{z}, \mu_F^2\right). \tag{171}$$

2. **Singlet Sector ($\Sigma(x,\mu_F^2) = \sum_{i=1}^{n_f}[q_i(x,\mu_F^2) + \bar{q}_i(x,\mu_F^2)]$ and $g(x,\mu_F^2)$):**

   Forms a coupled 2×2 system describing quark-gluon mixing:

$$\frac{\partial}{\partial \ln\mu_F^2} \begin{pmatrix} \Sigma(x,\mu_F^2) \\ g(x,\mu_F^2) \end{pmatrix} = \frac{\alpha_s(\mu_F^2)}{2\pi} \int_x^1 \frac{dz}{z} \begin{pmatrix} P_{qq}(z) & 2n_f P_{qg}(z) \\ P_{gq}(z) & P_{gg}(z) \end{pmatrix} \begin{pmatrix} \Sigma(x/z,\mu_F^2) \\ g(x/z,\mu_F^2) \end{pmatrix}. \tag{172}$$

Leading-Order Splitting Functions The leading-order (LO) Altarelli-Parisi splitting kernels are:

$$P_{qq}(z) = C_F\left[\frac{1+z^2}{(1-z)_+} + \frac{3}{2}\delta(1-z)\right], \tag{173}$$

$$P_{qg}(z) = T_F\left[z^2 + (1-z)^2\right], \tag{174}$$

$$P_{gq}(z) = C_F\left[\frac{1+(1-z)^2}{z}\right], \tag{175}$$

$$P_{gg}(z) = 2C_A\left[\frac{z}{(1-z)_+} + \frac{1-z}{z} + z(1-z)\right] + \frac{11C_A - 2n_f}{6}\delta(1-z). \tag{176}$$

Soft gluon divergences at $z \to 1$ are regularized via the plus-distribution:

$$\int_0^1 \mathrm{d}z \frac{g(z)}{(1-z)_+} \equiv \int_0^1 \mathrm{d}z \frac{g(z)-g(1)}{1-z}. \tag{177}$$

PDF fits PDFs have to be determined from data. Many aspects:

- Perturbative order
- Higher twist
- Resummation
- Heavy mass flavour scheme
- Parametrisation
- Fitting scale
- Treatment of missing higher order uncertainties
- Electroweak parameters + corrections
- Quark masses
- Evolution settings
- Fitting technique

4.5 Collinear Factorization in hadron-hadron collisions

At hadron colliders such as the LHC, cross sections for the production of a final state Y (we will be interested in $Y = VV$ boson pair production or $Y = VVjj$ VBS/VBF) factorize into universal non-perturbative Parton Distribution Functions (PDFs) and infrared-safe partonic hard-scattering cross sections:

$$\mathrm{d}\sigma_{pp\to Y+X} = \sum_{a,b} \int_0^1 \mathrm{d}x_1 \mathrm{d}x_2\, f_a(x_1, \mu_F^2)\, f_b(x_2, \mu_F^2)\, \mathrm{d}\hat{\sigma}_{ab}(x_1, x_2, \mu_R^2, \mu_F^2), \tag{178}$$

where μ_F and μ_R denote the factorization and renormalization scales. The partonic cross section is perturbatively expanded in powers of the strong coupling $\alpha_s(\mu_R)$:

$$\mathrm{d}\hat{\sigma}_{ab} = \mathrm{d}\hat{\sigma}_{ab}^{(0)} + \underbrace{\mathrm{d}\hat{\sigma}_{ab}^{(1)}}_{\mathcal{O}(\alpha_s)} + \underbrace{\mathrm{d}\hat{\sigma}_{ab}^{(2)}}_{\mathcal{O}(\alpha_s^2)} + \dots \tag{179}$$

The leading-order cross section is described by the Born matrix element

$$d\hat{\sigma}_{ab}^{(0)} = d\hat{\sigma}_{ab}^{\mathrm{B}} = \frac{1}{2\hat{s}} \frac{1}{N_{ab}} \mathrm{d}\Phi_Y\, \langle \mathcal{M}_{ab\to Y}^{(0)} | \mathcal{M}_{ab\to Y}^{(0)} \rangle (\Phi_Y) \mathcal{F}(\Phi_Y)\ . \tag{180}$$

Here we denote $\hat{s} = x_1 x_2 s^{\mathrm{had}}$ as the partonic center of mass energy. We also introduce our notation for squared matrix elements $\langle \mathcal{M}_{ab\to Y}^{(0)} | \mathcal{M}_{ab\to Y}^{(0)} \rangle$ which imply sums over all external polarizations and colors as well as the "measurement function" $\mathcal{F}(\Phi_Y)$ which describes the observable of interest and can be used to implement phase space cutoffs and/or histograms.

The scattering amplitudes $|\mathcal{M}_{ab\to Y}\rangle$ can be calculated from perturbation theory and also obey a perturbative expansion:

$$|\mathcal{M}_{ab\to Y}\rangle = |\mathcal{M}_{ab\to Y}^{(0)}\rangle + |\mathcal{M}_{ab\to Y}^{(1)}\rangle + |\mathcal{M}_{ab\to Y}^{(2)}\rangle + \dots \tag{181}$$

Acknowledgements

I would like to acknowledge the inspiration and input from various lectures on precision phenomenology at HEP schools, as well as standard QCD textbooks (citations in the main text). In particular, I build on the excellent QCD lectures by Giulia Zanderighi, Nigel Glover, and Gavin Salam.

References

[1] John C. Collins. *Renormalization : An Introduction to Renormalization, the Renormalization Group and the Operator-Product Expansion*. Vol. 26. Cambridge Monographs on Mathematical Physics. Cambridge: Cambridge University Press, 1984. ISBN: 978-0-521-31177-9. DOI: 10.1017/9781009401807.

[2] Michael E. Peskin and Daniel V. Schroeder. *An Introduction to quantum field theory*. Reading, USA: Addison-Wesley, 1995. ISBN: 978-0-201-50397-5. DOI: 10.1201/9780429503559.

[3] R. Keith Ellis, W. James Stirling, and B. R. Webber. *QCD and collider physics*. Vol. 8. Cambridge University Press, Feb. 2011. ISBN: 978-0-511-82328-2. DOI: 10.1017/CBO9780511628788.

[4] John Collins. *Foundations of Perturbative QCD*. Vol. 32. Cambridge University Press, 2011. ISBN: 978-1-009-40184-5. DOI: 10.1017/9781009401845.

[5] ATLAS Collaboration. "Standard Model summary plots - July 2026". In: *Preprint* (2026).

[6] Albert M Sirunyan et al. "Measurement of differential cross sections for the production of top quark pairs and of additional jets in lepton+jets events from pp collisions at $\sqrt{s} = 13$ TeV". In: *Phys. Rev. D* 97.11 (2018), p. 112003. DOI: 10.1103/PhysRevD.97.112003. arXiv: 1803.08856 [hep-ex].

[7] S. Catani and M. H. Seymour. "A General algorithm for calculating jet cross-sections in NLO QCD". In: *Nucl. Phys. B* 485 (1997). [Erratum: Nucl.Phys.B 510, 503–504 (1998)], pp. 291–419. DOI: 10.1016/S0550-3213(96)00589-5. arXiv: hep-ph/9605323.

[8] S. Frixione, Z. Kunszt, and A. Signer. "Three jet cross-sections to next-to-leading order". In: *Nucl. Phys. B* 467 (1996), pp. 399–442. DOI: 10.1016/0550-3213(96)00110-1. arXiv: hep-ph/9512328.

[9] Michał Czakon et al. "Single-jet inclusive rates with exact color at $\mathcal{O}(\alpha_s^4)$". In: *JHEP* 10 (2019), p. 262. DOI: 10.1007/JHEP10(2019)262. arXiv: 1907.12911 [hep-ph].